

ITTC2024

**30TH INTERNATIONAL TOWING TANK CONFERENCE
22–27 SEPTEMBER 2024 | HOBART TASMANIA AUSTRALIA**

Report of the Specialist Committee on Ocean Renewable Energy

SPECIALIST COMMITTEE ON OCEAN RENEWABLE ENERGY

1. INTRODUCTION

This report summarizes the work of the Specialist Committee on Ocean Renewable Energy for the 30th ITTC.

1.1 Membership and Meetings

The members of the Specialist Committee on Ocean Renewable Energy of the 30th ITTC has been organized into three focus group: Offshore wind turbines (OWT), current turbines (CT), and wave energy converters (WEC).

The committee consisted of the following members, divided into their respectively focus group:

Offshore Wind Turbines (OWT):

- Prof. Maurizio Collu (Chair)
University of Strathclyde,
Glasgow
UK
- Dr. Petter Andreas Berthelsen (Secretary)
SINTEF Ocean,
Trondheim
NORWAY
- Dr. Vincent Leroy
École Centrale de Nantes,

Nantes
FRANCE

- Prof. Antonio Fernandes
LOC/COPPE/UFRJ,
Rio De Janeiro,
BRAZIL
- Dr. Weiwen Zhao
Shanghai Jiao Tong University,
Shanghai
P.R. CHINA

Wave Energy Converters (WEC):

- Prof. Motohiko Murai
Yokohama National University,
Yokohama
JAPAN
- Dr. Giuseppina Colicchio
CNR-INM,
Rome
ITALY
- Dr. Kyong-Hwan Kim
KRISO,
Daejeon,
KOREA

Current Turbines (CT):

- Prof. Gustavo R. S. Assi
University of São Paulo,
São Paulo,
BRAZIL
- Dr. Jean-Roch Nader
Australian Maritime College,
Launceston,

TASMANIA

Four committee meetings have been held during the work period:

- Online, 9-11 November 2021.
- Online, 23-25 August 2022.
- University of Strathclyde, Glasgow, UK, 9-11 May 2023.
- Online, 9-11 January 2024.

1.2 Acknowledgements

The Committee would also like to acknowledge the contributions of Christopher Vogel, and Rodrigo Batista Soares.

1.3 Tasks

The recommendations for the work of the Specialist Committee on Ocean Renewable Energy as given by the 29th ITTC were as follows:

1.3.1 General recommendations

- Continue interactions with IEC.
- Review interactions between model scale and moderate/full scale test sites.
- Review of testing of deployment (transportation, installation) and O&M for marine renewable devices.
- Review testing of multipurpose platforms (e.g., combined WEC/OWT/ Solar/Aquaculture platforms).

1.3.2 Recommendations for wave energy converters (WECs)

- Continue to monitor development of new concepts of WECs.
- Continue to monitor developments in PTO modelling both for physical and numerical prediction of power capture.

- Assess the feasibility of developing specific guidelines for numerical and experimental survival testing of WECs.
- Assess support to using the benchmark round robin data for numerical comparison and/or for evaluating facility biases and scale related uncertainties.
- Update the uncertainty analysis of WEC testing to include the uncertainties of the power capture and potentially of a different type of device technology.
- Update and extend array section of the guidelines for numerical modelling of WECs.
- Review and report on the different PTO control strategies for power optimization and survivability modes.
- Review and report on comparisons between full scale data and numerical work/experimental model testing.

1.3.3 Recommendations for current turbines (CTs)

- Continue to monitor development in physical and numerical techniques for prediction of performance of current turbines
- Assess the support for round robin test of a 3-blade horizontal axis turbine (such as the DoE turbine). If there are enough willing participants develop a technical delivery plan.
- Review and report the techniques use for CFD modelling current turbines. This should include the use of combined EFD/CFD techniques for scaling and blockage corrections and methodologies for replicating environmental conditions.

1.3.4 Recommendations for offshore wind turbines (OWTs)

Continue monitoring and report on the development in full-scale installation of floating offshore wind turbines.

Report on possible full-scale measurement data available and address how these data can be

utilized for validation of simulation tools and evaluation of scaling effects from model scale tests.

Continue monitoring and report on the development in model testing methodology for offshore wind turbines.

- Review and report on recent development of physical wind field modelling in open space with application for wave tank testing of floating offshore wind turbines, including modelling of turbulence and measuring and documentation of the wind field.
- Review and report on the development of numerical offshore wind farm modelling.

2. PROCEDURES AND GUIDELINES

2.1 Existing guidelines

This committee is responsible for maintaining the following ITTC procedures and guidelines:

- 7.5-02-07-03.7 Wave Energy Converter Model Test Experiments

This procedure addresses designing and performing hydrodynamic model tests of wave energy converters. The guideline provides a careful consideration of the differences and complexities in testing a device at various TRLs where for example the power take-off (PTO) system should be representative of the full-scale PTO and survivability tests where extreme load fatigue analysis is required. No major revision has been performed during the 29th ITTC.

- 7.5-02-07-03.8 Model tests for Offshore Wind Turbines

This procedure addresses designing and performing hydrodynamic model tests of offshore wind turbines. The guideline describes different methods for modelling of the wind loads on the wind turbine in a hydrodynamic testing facility as well as test procedures for offshore wind turbines. No major revision has been performed

during the 30th ITTC, but in addition to a general polishing and minor updates, the acronym list has been revised and the list of symbols has been added.

- 7.5-02-07-03.9 Model tests for Current Turbines

This procedure involves the design and execution of model tests for ocean and tidal current turbine devices across a range of scales in a reproducible environment, specifically at a hydrodynamic test facility. The primary objective is to assess the suitability of this facility for conducting comprehensive tests on ocean and tidal current turbine devices, ensuring accurate and reliable results. The procedure was revised to ensure conformity and consistency across ITTC guidelines. This revision has not introduced any new sections. Some sentences have been rewritten for clarity.

- 7.5-02-07-03.12 Uncertainty Analysis for a Wave Energy Converter

The procedure addresses guidelines for the application of uncertainty analysis to the small-scale testing of wave energy converters provided by ITTC procedure 7.5-02-07-03.7, “Wave Energy Converter Model Test Experiments”. Details about the energy capture performance have been added to the procedure. Because of the relative importance of the PTO system in the different stages of development, three macro categories for the applications of the uncertainty have been identified: the concept validation stages (TRL 1-3), the design validation stages (TRL 4-5) and the system validation, prototype, and demonstration stage (TRL 6-9). For each of these stages, the sources of uncertainty to consider are listed as well as guidelines for their reliable evaluation.

- 7.5-02-07-03.15 Uncertainty Analysis – Example for horizontal-axis current turbines

The procedure addresses guidelines for applying uncertainty analysis to the small-scale testing of horizontal-axis current turbines provided by ITTC procedure 7.5-02-07-03.9, “Model Tests for Current Turbines”. The guideline was revised for consistency, and some sentences were rewritten for clarity. Brief comments have been added on the uncertainty analysis for unsteady experiments as well as experiments with arrays of turbines in proximity (high blockage). The equations have been revised and corrected where necessary. The title of the document should be updated to “Uncertainty Analysis - Example for Horizontal-Axis Current Turbines”.

- 7.5-02-07-03.17 Uncertainty Analysis for Model Testing of Offshore Wind Turbines

The purpose of the guideline is to provide guidance on the application of uncertainty analysis to the model scale testing of offshore wind turbines following the ITTC Procedure 7.5-02-07-03.8, “Model Tests for Offshore Wind Turbines”. The model scale testing of offshore wind turbines focuses on the environmental loads and global response of the structure, similar to the testing of other offshore structures (floating or fixed). The section on uncertainty has been substantially revised, adding the GUM approach for evaluating and expressing uncertainty (and its limitation), and a section on the Monte Carlo approach.

- 7.5-02-07-03.18 Practical Guidelines for Numerical Modelling of Wave Energy Converters

The purpose of this guideline is to provide a methodology to assess the fidelity of the numerical simulation for Wave Energy Converters (WECs) at different stages of development, to set up numerical calculations and to analyse the obtained results. Therefore, they have been classified as a function of the objectives of the study, of the Technology Readiness level (TRL) of the WEC and the numerical facility on which they can be run has been detailed.

2.2 New guidelines

No new guidelines were developed during this term.

For the WEC focus group, it was suggested to “Assess the feasibility of developing specific guidelines for numerical and experimental survival testing of WECs”. It was discussed and agreed that the best course of action is, rather than developing a new guideline, to update and extend 7.5-05-07-03.7, section 2.7.4, and 7.5-05-07-03.18, section 2.5 (see relevant info in section 2.1).

3. COOPERATION WITH OTHER COMMITTEES

3.1 Collaboration with the International Electrotechnical Commission (IEC)

3.1.1 Description

The IEC is a key international body which addresses standards in all field of electrotechnology. The work is organized through technical committees (TCs). The TC of relevance for the ITTC SC on ORE are IEC TC88 (Wind Turbines) and IEC TC114 (Marine Energy – Wave, tidal and other water current converters).

3.1.2 Meetings and workshop

Through the previous ITTC term, an official type A liaison with the has been established with the IEC TC114, and Prof. Maurizio Collu (SC ORE chair) has been nominated to cover this role in March 2022. During the 29th ITTC term, at the IEC TC114 plenary meetings of March 2022 and April 2023, the ITTC SC on ORE chair presented the ITTC in general, and the aims and scope of the ITTC SC on ORE. This has been followed by a meeting between two chairs (IEC TC114 and ITTC SC on ORE) to define a collaboration strategy between the two committees, and a copy of the IEC TS 62600-103 Ed. 1 (WEC) and of the IEC TS 62600-202 Ed. 1 (CT)

has been obtained, to be compared with the relevant procedures and guidelines of the present SC.

Furthermore, Dr. Thomas Davey, a member of the IEC TC114, has attended the 3rd committee meeting of the ITTC SC on ORE in Glasgow (May 2023). During this meeting, the work of the ITTC SC on ORE on WEC and CT has been presented more in details, and an approach to identify conflicts between ITTC procedures and guidelines and IEC guidelines has been defined.

3.1.3 Procedure to identify conflicts defined and trialed

The WEC and CT focus groups have performed a first pass at applying the approach defined to identify these conflicts comparing, respectively, the IEC TS 62600-103 Ed.1 vs 7.5-02-07-03.7 Wave Energy Converter Model Test Experiments, and IEC TS 62600-202 Ed. 1 vs 7.5-02-07-03.8 Model tests for Offshore Wind Turbines, and the work needs to be continued in the next term.

The chair of the ITTC SC on ORE is also working on establishing a type A liaison with the IEC TC88, which focusses on Offshore Wind Turbines, to apply the same approach.

4. STATE OF THE ART

4.1 Review of testing of deployment (transportation, installation) and O&M for OWT and WEC

4.1.1 Offshore wind turbines

Experimental and numerical testing, in the open literature, remains largely focused on operational and survival design load conditions for a fully installed and commissioned offshore wind turbines, although a few publications are starting to appear, illustrating the methodologies and results of investigations focused on deployment and maintenance phases.

Hyland et al. (2014) performed experimental towing tests analyses of the GICON TLP configuration, considering several operational and towing conditions – and observing Vortex-Induced Motion (VIM).

Buttner et al. (2022) performed an experimental analysis on the towing process of the Orthospar platform, subject to wave loads with different incoming directions, focusing on the towing line load imposed on the platform. Mas-Soler et al. (2021) experimentally investigated a Tension Leg Platform (TLP) towing characteristics, considering different towing configurations, both in calm water and under wave loads.

Le et al. (2021) investigated numerically and experimentally the dynamic response of two TLP configurations having a semisubmersible configuration during towing, measuring heave, pitch and roll under different significant heights. Bollard pull requirements for different towing scenarios are also investigated. More recently, Ramachandran et al. (2024) conducted a comprehensive experimental and numerical study on towing operations of the DeepCwind semisubmersible platform, highlighting the importance of the evaluation of viscous forces in numerical models, and other non-linear phenomena, such as VIM, fishtailing, galloping, and pitch-induced wave run-up, observed in the experiments.

4.1.2 Wave energy converters

Wave energy is not necessarily at a higher Technology Readiness Level (TRL) than other renewable energy sources. Research and development in this field is progressing rapidly, and new, more efficient devices are constantly being developed. It is estimated that more than 1,000 patents for wave energy converter (WEC) concepts have been granted annually worldwide, and thousands of existing patents have been registered. This indicates that WEC designs have not yet converged into a single type.

Existing WECs can be broadly classified into three types based on their basic operating

principles: "overtopping devices", "oscillating bodies", and "oscillating water columns". Recently, point-absorption wave energy conversion devices, which are a type of oscillating body, have been attracting attention due to their relatively easy construction and expected lower overall cost if deployed in a wave energy farm.

The development of numerical techniques and tank testing to validate them are important for WEC R&D, which is still under development. Numerical and experimental test cases have been devised by the International Energy Agency's Ocean Energy Systems (IEA OES) in its Task 10 "Wave Energy Converters Modelling Verification and Validation", presenting comparisons among linear, weakly nonlinear, and fully nonlinear codes, as well as experimental data.

The latest open-source software for WEC simulation is the WEC-Sim series, developed in MATLAB/SIMULINK using the multi-body dynamic solver Simscape Multibody. The project team is planning to develop a code to obtain the hydrodynamic coefficients needed for the pre-processing of WEC-Sim based on the Boundary Element Method.

The European project MaRINET2, a network of 39 partners in 13 European countries, has been working to progress offshore renewable energy technologies such as wave, tidal, and offshore wind. The project focused on testing two kinds of WECs to identify the uncertainty deriving from facility bias, but no further updates on its progress have been publicized after 2019.

Similarly, the pan-European COST action WECANET had planned another round-robin test to contribute to large-scale WEC array deployment, but no further updates on its progress have been published after 2021.

Papers on numerical simulation of wave power generation have been published extensively, likely due to the proliferation of open-source codes and general-purpose software,

which make it easier to obtain numerical solutions at a certain level. These include studies on arrays of more than 10 WECs, as well as the use of AI models to predict waves, motion, and control forces. However, different types of WEC technologies have different issues, and the validation of numerical models remains challenging in some respects.

In summary, while a great number of new ideas have emerged in wave power generation, and numerical calculations and tank experiments have been conducted on them, most are still commercially immature and not yet fully verified through numerical analysis, tank tests using scaled models, and intercomparisons of demonstration projects using full-scale devices. Developing basic tank test data that can validate numerical analyses may be necessary to advance the field.

4.2 Review testing of multipurpose platforms (MPPs)

While multi-purpose platforms (MPPs) hold great potential for the offshore industry, their technological readiness level is very low, requiring comprehensive experimental trials. These trials are usually complex due to the need to integrate various subsystems, each governed by its own set of physical laws.

Wan et al. (2016) conducted a comparative experimental study on the survivability of a combined wind-wave floating offshore energy converter, the spar-torus combination (STC), testing three possible survival strategies against extreme loads. The study described the two model tests and compared the measured responses for each survival mode. Sarmiento (2019) performed experimental testing of a wind-wave MPP floating platform, providing insights into its global response, mooring loads, and the performance of the integrated oscillating water column wave converters under different sea states. The wind turbine was simulated using a wind generator and a drag disk, while the

OWC dynamics were reproduced through different diameter openings.

Ruzzo et al. (2021) reviewed the scaling laws and strategies for physical modeling of MPPs, highlighting the higher conflicts of a Froude-scaling approach when considering different subsystems, and the limitations of small-scale modeling due to the generally larger size of MPPs. Modeling the forces on flexible aquaculture nets poses a substantial challenge, as aquaculture is often integrated into these platforms.

Konispoliatis (2021) proposed a TLP-type renewable energy multi-purpose (wind-wave) floating offshore system and conducted scaled-model experiments to validate the analytical and numerical models developed, focusing on the hydrodynamic aspects. Ohana et al. (2023) described an experimental campaign aimed at assessing the coupled dynamics of a wind-wave-aquaculture MPP and providing data for

numerical models' validation. The tests were carried out with a 1:40 model in a large ocean basin, with the wind turbine represented using a Software-In-The-Loop approach. Ruzzo et al. (2023) presented an experimental set-up for an outdoor, field campaign on a 1:15 scale wind-wave-aquaculture MPP, including a large moonpool, over 11 months. The study provided details on the scaled platform, measurement systems, and data acquisition for various parameters.

4.3 Full-scale installations

4.3.1 Current turbines

Table 1 lists full-scale deployed or planned projects in the last five years (2018-2023). Very little information regarding long-term project survivability is available.

Table 1 Active current turbine projects deployed or planned between 2018 and 2023. Database collected and published by the PRIMRE Portal and Repository for Information on Marine Renewable Energy (<https://openei.org/wiki/PRIMRE>)

#	Start Year	Project Name	Project Manager	Country	Capacity (MW)	Project Scale	Devices	Number of Devices	Waterbody
1	Planned	FloWatt	Hydroquest SAS,Qair	France	17.5	Array	Hydroquest	7	Le Raz Blanchard, Normandie, France
2	Planned	MeyGen Pentland Firth Phase 2	SIMEC Atlantis Energy	United Kingdom	312	Array	Seagen S		Inner Sound of the Pentland Firth
3	Planned	Morecambe Bay and Duddon Estuary Tidal Lagoon	North West Energy Squared Limited,Northern Tidal Power Gateways	United Kingdom	3960	Array		132	Morecambe Bay and the Duddon Estuary, Irish Sea
4	Planned	Morlais	Menter Mon	United Kingdom	240	Array	O2 Turbine, Magallanes Renovables ATIR, Nova M100		Irish Sea, Wales, United Kingdom
5	Planned	SBS 1MW Pilot Project	SBS Intl Ltd	Indonesia	1	Array			
6	Planned	Uisce Tapa Project	DP Energy,Halagonia Tidal Energy Ltd	Canada	9	Array	HS1500	6	Minas Passage, Bay of Fundy, Atlantic Ocean
7	2022	Larantuka 10MW project	SBS Intl Ltd	Indonesia	10	Array			Larantuka Strait, Indonesia

8	2022	Pemba, Açık In-stream Tidal Energy Project	Sustainable Marine Energy Ltd, Fundy Ocean Research Center for Energy	Canada	9	Array	PLAT-I	20	Bay of Fundy, Nova Scotia, Canada
9	2022	Vestmanna Tidal Power Plant	Minesto AB	Denmark	1.4	Array	Minesto Dragon 4, Minesto Dragon 12	3	Vestmanna, Faroe Islands
10	2021	East Foreland Tidal Project	Ocean Renewable Power Company	United States	5	Array	Seagen S		Cook Inlet
11	2021	Green Hydrogen and Oxygen Supply from Tidal Energy	Nova Innovation Ltd	United Kingdom	3	Array	Nova M100	30	Yell, Scotland, United Kingdom
12	2021	Islay Community Demonstration	Flex Marine Power Ltd	United Kingdom	0.05	Single Device	FM-Swimmer Tidal Turbine	1	Sound of Islay, Scotland, United Kingdom
13	2021	Kootznahoo Inlet	Littoral Power Systems Inc, Barrett Energy Resources Group	United States	0.3	Single Device		1	Kootznahoo Inlet, AK, USA
14	2021	Orbital at PTEC	Scotrenewables	United Kingdom	15	Array	O2 Turbine	7	Isle of Wright, United Kingdom
15	2021	Perpetuus Tidal Energy Centre PTEC	Perpetuus Tidal Energy Centre Ltd	United Kingdom	30	Array	O2 Turbine		South coast of the Isle of Wight
16	2021	West Somerset Tidal Lagoon	Halcyon Tidal Power LLC	United Kingdom	3000	Array		960	Bristol Channel
17	2020	FORWARD2030	Scotrenewables	United Kingdom	10	Array	O2 Turbine	2	Fall of Warness, Scotland, United Kingdom
18	2020	Lashy Sound Phase 2	Orbital Marine Power	United Kingdom	20	Array	O2 Turbine	10	Lashy Sound, Orkney; Scotland, Orkney
19	2020	MeyGen Pentland Firth Phase 1b	SIMEC Atlantis Energy	United Kingdom	10	Array	Seagen S	6	Inner Sound of the Pentland Firth
20	2019	Blue Shark Power Djibouti 2	Blue Shark Power System	Djibouti	120	Array	Blue Shark	495	
21	2019	FORCE 9 MW Pre-Commerical Demo	ANDRITZ Hydro	Canada	9	Array	HS1500	6	Minas Basin
22	2018	Grand Passage	Sustainable Marine Energy Ltd	Canada	0.7	Single Device	PLAT-I	1	Grand Passage, Nova Scotia, Canada
23	2018	Holyhead Deep	Minesto AB	United Kingdom	80	Array	Deep Green Tidal Kite	20	Irish Sea, UK
24	2018	Majis	New Energy Corporation	Oman	0.005	Array			Port of Sohar, Oman

25	2018	MeyGen Pentland Firth Phase 1c	SIMEC Atlantis Energy	United Kingdom	6	Array	SIMEC AR1500, ANDRITZ Hydro HS1000	4	Inner Sound of the Pentland Firth
26	2018	P154 Guinard Demo	Guinard Energies Nouvelles	France	0.02	Single Device	MegaWattBlue	1	Atlantic Ocean
27	2018	Vestmanna DG100 Tidal Kite System	Minesto AB	Denmark	0.1	Array	Deep Green Tidal Kite		Vestmanna, Faroe Islands

4.3.2 Offshore wind turbines (Floating)

The global offshore wind industry has seen significant growth from 2021 to 2024. In 2021, the cumulative global offshore wind installed capacity grew to 50,623 MW from 257 operating projects, largely driven by China's commissioning of 13,790 MW. The size of offshore wind turbines has also increased, with the

world's largest single-capacity 16 MW turbines now in operation in China. Floating offshore wind turbines have also seen progress, with the total installed capacity reaching 57.1 MW in 2021, including the largest floating offshore wind project in the UK and several demonstration projects in China. However, there are still many challenges to overcome, such as fully coupled performance analysis and lightweight design for cost reduction.

Table 2 List of floating offshore wind farm projects

PROJECT NAME	COUNTRY	COMMISSIONING	CAPACITY (MW)	OWNER
TetraSpar Demo	Norway	2021	3.8	Stiesdal
Three Gorges Leader Demo (Sanxia YingLing Hao)	China	2021	5.5	China Three Gorges
Haizhuang Fuyao Demo	China	2022	6.2	CSSC Haizhuang
Haiyou Guanlan Demo	China	2023	7.25	CNOOC
Hywind Tampen Norway	Norway	2023	88	Equinor
Les éoliennes flottantes du Provence Grand Large (PGL)	France	2024	24	SBM Offshore
Forthwind Demo	UK	2024	20	#N/A
Mingyang OceanX Demo	China	2024	16.6	Mingyang
EOLMed	France	2025	30	Ideol
Les éoliennes flottantes du Golfe du lion (EFLG)	France	2025	30	Principle Power
Pentland Deom (Dounreay Tri)	UK	2025	15	#N/A
Hainan Wanning Offshore Floating Phase I	China	2025	200	Power China
Flocan 5 Canary	Spain	2025	25	Grupo Cobra
Goto Sakiyama Oki Oki Huangdao Pilot A	Japan	2026	16.8	Toda
Goto Sakiyama Oki Oki Huangdao Pilot B	Japan	2026	5.2	Toda
Hainan Wanning Offshore Floating Phase II	China	2027	800	Power China

Oahu North, Hawaii	USA	2032	400	Principle Power
Oahu South, Hawaii	USA	2032	400	Principle Power

4.3.3 Wave energy converters

Worldwide, WEC full-scale tests are continuing, with wave power generation units of tens of kW to MW being developed. Most WECs are movable or OWC types, with full-scale deployments mainly in Europe and recent activity in the US and Asia. However, information on full-scale tests is limited, and meaningful power

generation for commercialization has not been achieved. Overcoming survival at sea remains a key challenge, as it is directly related to cost and a barrier to commercialization. While full-scale tests are increasing, and the IEC is preparing a performance evaluation system, more disclosure of test information and technical progress is needed to advance the wave energy sector.

Table 3 List of the recent projects on WECs

PROJECT NAME	COUNTRY	YEAR ONLINE	DEVELOPMENT STATUS	DEVELOPER	Scale	RATED POWER [MW]	TYPE
LAMWEC	Belgium	2020/2021	At Sea Prototype	Laminaria	1:7	0.2	Point Absorber
Wavepiston	Denmark	2017-2019	Demonstration Scale	Wavepiston A/S	Full Scale	Unknown	Oscillating Wave Surge Converter
mWave	Wales	2021	Development	Bombora	1:7	1.5	Gravity Based Pressure Differential
King Island Project	Australia	2020	Installed Waiting Connection	Wave Swell Energy	Full Scale	0.2	Oscillating Water Column
OE Buoy	Ireland/USA	2020	Arrived at Hawaii Test Site	Ocean Energy (Ireland)	Full Scale	0.5	Oscillating Water Column
PowerBuoy	North Sea	2020	Operational	Ocean Power Technologies	Full Scale	0.003	Point Absorber
NEMOS Wave Energy Converter	Belgium	2019	At Sea Prototype	NEMOS	Large Scale	Unknown	Point Absorber
Tordenskiold	Denmark	2019	Half-Scale Open Sea	Crestwing	1:2	Unknown	Attenuator
WAVEGEM	France	2019	At Sea Prototype	GEPS Techno	Full Scale	0.15	Point Absorber
WaveSub	United Kingdom	2018	At Sea Prototype	Marine Power Systems	1:4	4.5 full scale (Prototype rated power unknown)	Submerged Point Absorber
WaveRoller	Portugal	2018	At Sea Prototype	AW-Energy	unknown	0.25	Oscillating Wave Surge Converter
C4	Sweden	2018	At Sea Prototype	CorPower	Full Scale	0.3	Point Absorber

PROJECT NAME	COUNTRY	YEAR ONLINE	DEVELOPMENT STATUS	DEVELOPER	Scale	RATED POWER [MW]	TYPE
Oneka Buoy	Canada	2018	At Sea Prototype	Oneka	unknown	5-10 m ³ of fresh water per day	Point Absorber
Penguin	Finland	2017	Grid Connected Test	Wello Oy	Full Scale	1	Internal Rotating Mass
Wanshan 1 MW (2x500 kW) Wave Energy Demonstration Project	China	2023	Under Construction	Guangzhou Institute of Energy Conversion (GIEC)	Full Scale	1	Oscillating Wave Surge Converter
Exowave WEC	Denmark	2022	Operational	Exowave	Small Scale	0.001	Oscillating Wave Surge Converter
Floating Power Plant A/S Commercial scale PTO dry test rig (PTO TWIN)	Denmark	2022	Under Construction	Floating Power Plant A/S	Full Scale	0.2	Point Absorber
DIKWE	France	2022	At Sea Prototype	Geps Techno/Groupe LE-GENDRE	1:4	Unknown	Oscillating Wave Surge Converter
REWEC3 @ Civitavecchia	Italy	2022	Operational	Mediterranean University of Reggio Calabria	Full Scale	0.02	Oscillating Water Column
Overtopping Breakwater (OBREC)	Italy	2022	Operational	University of Campania Luigi Vanvitelli	Full Scale	0.015	Wave Overtopping
ISWEC revamp	Italy	2022	Under Construction	ENI, Wave for Energy, Politecnico di Torino	Full Scale	0.25	Internal Rotating Mass
Youngsoo OWC Pilot Plant	Korea	2022	Operational	KRISO	Full Scale	0.5	Oscillating Water Column
OWC WEC with Breakwater	Korea	2022	Operational	KRISO	Full Scale	0.03	Oscillating Water Column
Mutriku Wave Power Plant	Spain	2022	Operational	EVE	Full Scale	0.296	Oscillating Water Column
Ocean Energy Buoy (OE Buoy)	USA	2022	Under Construction	Ocean Energy Ltd,	Full Scale	0.5	Oscillating Water Column
C-Power SeaRay Wave Power System (previously planned as StingRAY WEC)	USA	2022	Under Construction	C-Power	Full Scale	0.02	Oscillating Wave Surge/Heave Converter
Blue X	UK	2022	Operational	Mocean Energy	Full Scale	0.01	Attenuator

* Note: from the IEA OES Annual Report 2021, 2022 and 2023

4.4 Wave energy converters

4.4.1 New concepts

WECs can be categorized by the physical process used to extract energy (Falcão (2010)): "Oscillating Water Columns", "Oscillating bodies", and "Overtopping devices". Recent trends in numerical studies explore introducing AI techniques, such as machine learning, into control algorithms to improve efficiency. However, it is challenging to scale down and test the power take-off (PTO) mechanisms used in actual equipment. Examples include using AC control systems and simulating PTO systems for OWC and other pneumatic equipment using orifice loads during proof-of-concept testing to overcome this challenge.

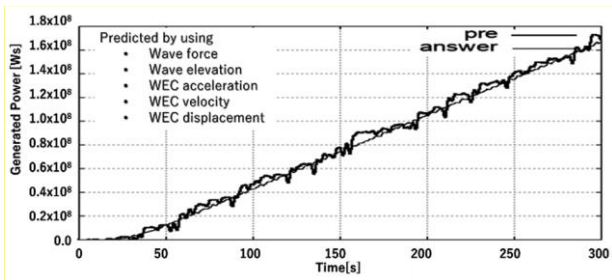


Figure 1: Comparisons of accumulated power generation: analytical result VS AI model (M. Murai, (2022))

4.4.2 Power take-off systems (PTO)

Scaling down and testing the power take-off (PTO) mechanisms used in actual wave energy converter (WEC) equipment is challenging. Examples include using AC control systems and simulating PTO systems with Coulomb or linear dampers, as well as simulating OWC and pneumatic PTO systems using orifice loads during proof-of-concept testing. The ITTC guideline 7.5-02-07-03.7 discusses various PTO systems for WEC model test experiments.

4.4.3 Physical and numerical modelling

Wave energy converter (WEC) problems often involve significant nonlinearities in fluid flow and fluid-structure/PTO interaction. However, for cases where the inviscid fluid hypothesis and small amplitude oscillations can be assumed, analytical solutions can be determined using the superposition principle to divide the problem into diffraction and scattering problems (Alves, 2016; Budan et al., 1975; Falnes et al., 1985). This allows the calculation of free surface oscillation, body motion, and potential hydrodynamic power extraction.

The ITTC guideline 7.5-02-07-03.18 Practical Guidelines for Numerical Modelling of Wave Energy Converters categorizes numerical modeling methods for WECs as potential flow models, CFD models, and hybrid models, providing considerations and a summary of the status and characteristics of each method in terms of Technology Readiness Level (TRL).

4.4.4 Control strategies

Recent years have seen an increase in numerical studies on the introduction of AI technologies, such as machine learning, into control strategies to improve wave energy converter (WEC) efficiency. Machine learning can be classified into methods like Deep Neural Network, Convolutional Neural Network, Recurrent Neural Network, and Long Short Term Memory. However, this classification may not remain appropriate as more branches and combinations of AI techniques continue to emerge for WEC applications.

4.4.5 Array of WECs

The hydrodynamic interactions between multiple WECs in a wave farm can significantly affect energy conversion. Incident waves are diffracted and refracted between devices, potentially reducing or increasing the total energy absorption of the WEC array.

The hydrodynamic interaction between WEC arrays is described by the multiple scattering model, as expressed by Kagemoto and Yue (1986). Within linear wave theory, this direct matrix model is considered rigorous. Li and Murai et al. (2018) evaluated the output performance of point absorber arrays, considering PTO copper losses. Their results showed that a transverse linear arrangement outperformed other configurations, with an optimal device spacing of around 50% of the significant wave period wavelength.

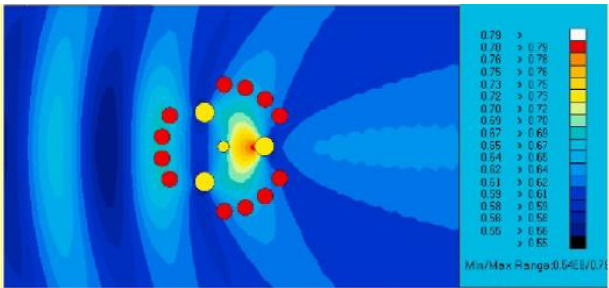


Figure 2: Wave forms around the DeepCwind semi-submersible with different PA-WECs arrangements (Hamid, R.G., et. al, (2021))

Potential flow theory cannot account for viscous effects such as boundary layer separation, turbulence, wave breaking, and wave overtopping. However, these phenomena are essential in predicting the hydrodynamic forces acting on the device. Therefore, CFD modelling based on the solution of the Navier-Stokes equations is starting to be employed. In recent years, the application of CFD methods to multi-point absorbing WECs has increased due to the rapid evolution of computational techniques. However, the computational cost is still too high to study arrays. At present, most CFD studies on multiple PA-WECs use finite volume methods, Li, et. al, (2012).

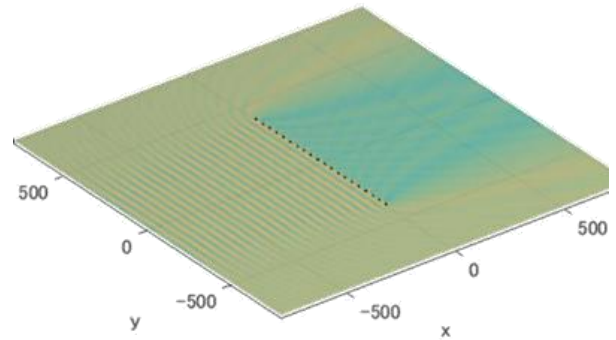


Figure 3: Example of the numerical simulation on arrayed 20 WECs and wave field around the array in regular waves (Murai et al, (2021))

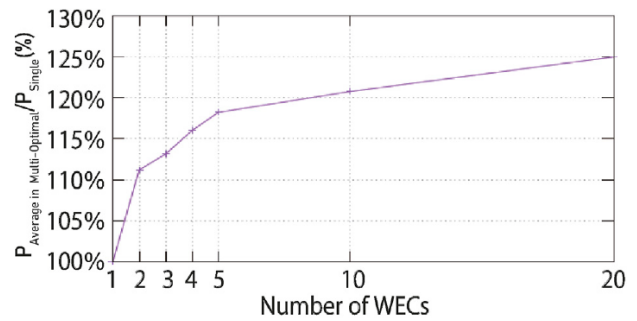


Figure 4: Increase rate of power generation of each PA-WEC number in the one direction irregular wave. (Murai et al, (2021))

Tank tests on arrays of multiple WECs can be broadly divided into cases where there is no common platform and cases where there is a common platform. In the former case, the focus is to optimize the layout configuration to maximize total output under different operating conditions, for example, considering regular or irregular waves and PTO system type. In the latter case, the focus is often on how the motion response of the platform is affected by controlling the WECs, for example, by assuming the attachment of multiple wave power generators to a floating wind turbine system.



Figure 5: Impression of a 2-WEC column array under regular waves, (V. Stratigaki, et al., (2014))



Figure 8: physical model Sketch of the wave basin (K. Sun, et al. (2021))

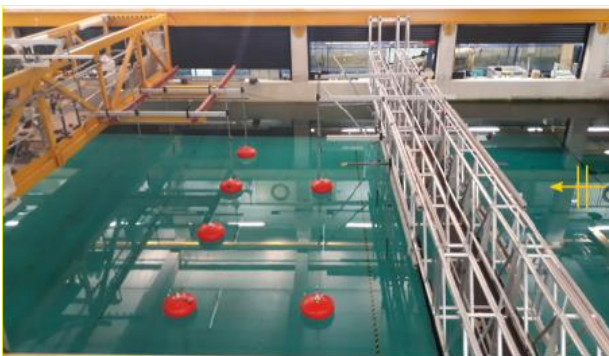


Figure 6: WECs' array layout (M. Giassi, et al., (2020))

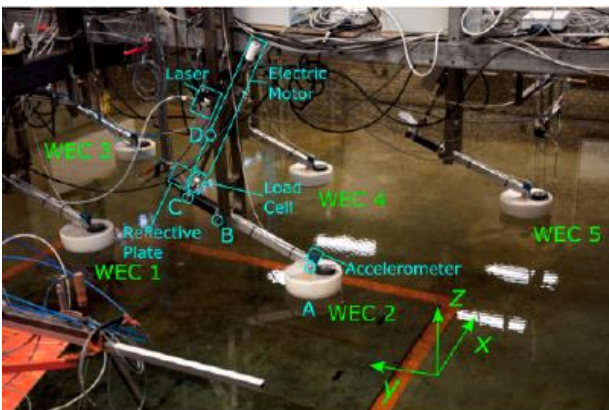


Figure 7: Model test (Mercadé et al.(2017))

4.5 Current turbines

4.5.1 Physical and numerical techniques for prediction of performance

The performance of hydrokinetic turbines is often predicted using semi-analytical approaches, computational fluid dynamics, machine learning, and experiments, at either model or full scale, depending on available test facilities, financial support, and scale factors.

4.5.1.1 Model Scale Measurements

Ensuring accurate representation of the investigated phenomenon is essential when conducting model-scale tests for wave energy converters (WECs) and hydrokinetic turbines. The model scale must be carefully chosen to accommodate geometric, kinematic, and dynamic similitudes while avoiding scale effects that could disrupt the output parameter values.

Guidelines and recommended practices, such as the ITTC guideline 7.5-02-07-03.9 and the IEC guideline (IEC, 2022), provide extensive recommendations for model tests, test facilities, result reporting, and factors to consider during analysis. Additionally, JCGM 100:2008 offers valuable advice on representing experimental uncertainties.

Model studies have exemplified tests to reach the performance of hydrokinetic turbines. Tests at the Federal University of Rio de Janeiro (UFRJ) by Fernandes & Rostami (2015) determined the efficiency of a Vertical Axis Autorotation Current Turbine (VAACT) under different Reynolds numbers and dimensionless moments of inertia. The results showed a maximum efficiency of approximately 7% at $Re=59,800$ and I^* in the range of 0.5-0.6 (Figure 9).

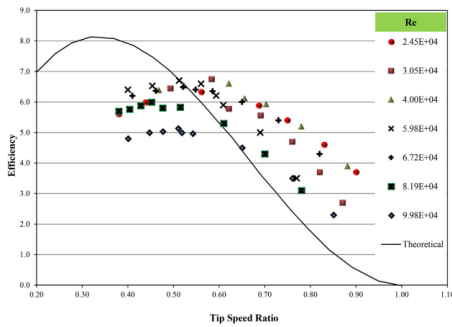


Figure 9: Experimental data for efficiency of flat plate model at $I^*=0.52$ (Fernandes & Rostami, 2015). The theoretical curve (black line) is reported by (Manwell et al., 2002)

Rostami and Fernandes (2015) further experimented on a flapped VAACT turbine, achieving a maximum efficiency of around 33% when the Reynolds number was 20,900 and the dimensionless moment of inertia was 0.70 (Figure 10).

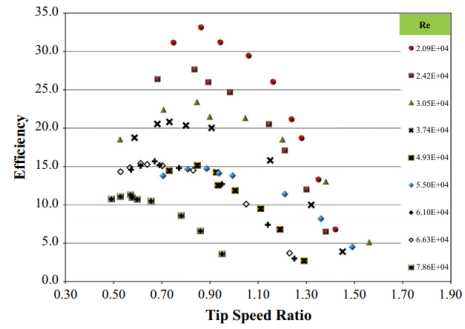
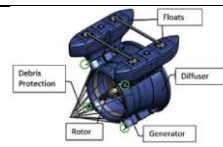
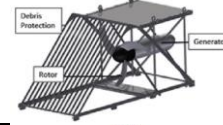





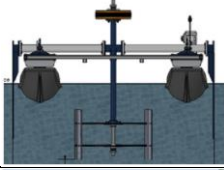



Figure 10: Experimental data for efficiency of flapped plate model at $I^*=0.70$ (Rostami & Fernandes, 2015)

4.5.1.2 In-Situ Measurements

In-situ measurements are a valuable practice that helps understand hydrokinetic turbines' performance and external loads. Even though these measurements come with high costs, they provide insights into any issues that may arise during the installation and operation of turbines. Typically, these measurements are conducted using devices with power capacities in the magnitude of kilowatts. Niebuhr et al. (2019) provide, in Table 4, examples of in-situ measurements and prototypes that have been installed and presented in the literature. Depending on the generator's characteristics and environmental constraints, these devices are placed near the free surface or at the riverbed.

Table 4: Developments with hydrokinetic turbine prototypes (Niebuhr et al., 2019)

Device	Characteristics	Picture
Smart Duofloat	Power Capacity: 5 kW Flow Velocity: 2.8 m/s Diameter: 1 m	
Smart Freestream	Power Capacity: 5 kW Flow Velocity: 3.1 m/s Diameter: 1 m	
Hydroquest River 1.4	Power Capacity: 40 kW Flow Velocity: 3.1 m/s	

Device	Characteristics	Picture
Waterrotor Energy Tech	Power Capacity: 1.1 kW Flow Velocity: 0.89 m/s	
Guinard Energies	Power Capacity: 130–3500 W Flow Velocity: 1 m/s	
EnviroGen Series	Power Capacity: 5 kW Flow Velocity: 3 m/s	
ORPC RivGen	Power Capacity: 15 kW Flow Velocity: 2.3 m/s	
HeliosAltas	Power Capacity: 100–500 W Flow Velocity: 1.8 m/s	
Instream energy system	Power Capacity: 25 kW Flow Velocity: 3 m/s	

4.5.1.3 Semi-Analytical Techniques

4.5.1.3.1 Blade Element Momentum (BEM) Theory

The blade element momentum theory is commonly used in designing horizontal axis turbines. This method divides the blades into two-dimensional sections to determine their torque and thrust. By integrating these properties along the blades, the total torque and thrust of the turbine can be calculated. BEM theory can be embedded in numerical codes for CFD simulations or numerical optimization (Yeo et al., 2022). It

is a popular choice for designing turbine blades to improve their performance curves and determine their design point (El-Shahat et al., 2020). Additionally, this technique is precious for exploring new concepts and designs (Elfering et al., 2023).

4.5.1.3.2 Actuator Disc Model

The actuator disc model utilizes the one-dimensional momentum theory. This involves applying simple hypotheses and conserving linear momentum to the control volume. However, specific corrections have been used to the model, such as incorporating wake rotation for horizontal axis turbines (Manwell et al., 2002).

The theory's most significant finding is the calculation of the maximum power coefficient versus the tip speed ratio (TSR). For the classic one-dimensional momentum theory model, the maximum power coefficient (C_p) is 59%, regardless of the tip speed ratio. However, the wake rotation model introduces a dependency on TSR, causing the curve to tend towards the maximum from the ideal model as TSR increases.

Recent advances in wind turbine aerodynamics have been made using the actuator disc model. (Bastankhah & Porté-Agel, 2014) have developed dynamic models that simulate lateral and vertical wake motion, known as dynamic wake meandering. Similarly, (Howland et al., 2019) have explored wind turbine wake steering strategies using the actuator disc model to optimize turbine yaw angles. Additionally, (Baratchi et al., 2020) have utilized the blade element actuator disc method in CFD for simulations with ducted tidal turbines. Finally, (Behrouzifar & Darbandi, 2019) employed this model to predict a horizontal axis turbine's performance and wake region.

4.5.1.3.3 Quasi-Steady Models

Quasi-steady models are widely used to predict turbine response and performance while minimizing time expenditure with simulations. This method relies on an equation of motion that depends on hydrodynamic coefficients derived from experiments or numerical simulations using a static turbine. These coefficients are determined based on the Reynolds number and angle of attack, and the resulting method can be an efficient alternative for research in this field.

Leroux et al. (2019) compared experimental results with computational fluid dynamics simulations using transient and quasi-steady models to simulate a horizontal axis turbine. The analysis focused on velocity deficits in the wake at distances of 2D, 3D, 6D, and 10D behind the turbine. Although the quasi-steady model did not predict the turbulence intensity distribution correctly and did not reflect wake behaviour

accurately, this model was consistent with experimental results for downstream distances greater than 6D (Figure 11).

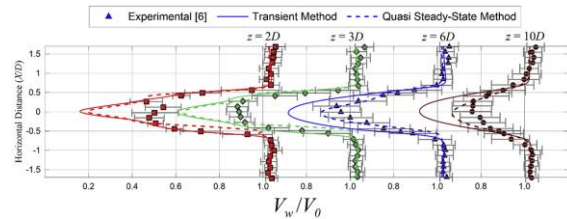


Figure 11: Normalized velocity comparison between experimental results and the transient-rotor simulation for the distance behind the turbine of 2D, 3D, 6D, and 10D (Leroux et al., 2019)

The stability, motions, and performance of flat plate turbines have also been explored in studies by (Fernandes & Mirzaeisefat, 2015; Mirzaeisefat & Fernandes, 2013; Soares et al., 2022b). These studies utilized numerical simulations to provide coefficients for the quasi-steady method to investigate turbine performance, showing that this methodology is feasible in studying hydrokinetic turbines.

Rostami & Fernandes (2017) performed an experimental and numerical study on the motion of flat plates in uniform flow. Their models showed excellent agreement, and the research indicated that a flat plate turbine performing fluttering must achieve a maximum efficiency of 19%. This efficiency is about 18% greater than that of autorotation.

4.5.1.4 Computational Fluid Dynamics (CFD)

One common method for simulating currents in turbines is to use computational fluid dynamics software. Typically, this involves a sliding-mesh approach, where the control volume is split into stationary and rotating regions. The rotating section includes the turbine geometry, which rotates with the turbine. Occasionally, remeshing techniques are used to generate a new mesh at each time step, but this is rare due to the high computational costs involved.

Turbulence models are used in CFD studies, and Reynolds numbers are usually in the turbulent range, making Direct Numerical Simulation impractical. Therefore, researchers focus on Reynolds-Averaged Navier-Stokes (RANS), Large Eddy Simulation (LES), and hybrid models like the Detached Eddy Simulation (DES). LES and DES models have good turbulence resolutions but require complex grid refinement. RANS models perform well with low grid refinement but fail to model high-gradient phenomena.

Kulkarni et al. (2022) reviewed CFD and Fluid-Structure Interaction (FSI) simulations to optimize tidal turbines. This technique allows researchers to determine how pressure and fluid flow affect structural deformations and how structural deformations affect pressure and flow.

The study by Niebuhr et al. (2022) on counter-rotating turbines employed the CFD technique to determine their performance and wake characteristics. To validate the rate of decay of turbulence intensity, the turbulence model was changed to decide which represented the wake characteristics more accurately (Figure 12). The experimental wake was compared to the results obtained from the turbulence models to interpret the BEM-CFD approach using RSM-LPS2. The findings revealed that the approach adheres closely to the experimental results and provides exemplary accuracy.

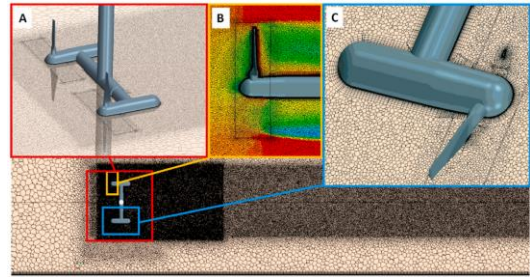


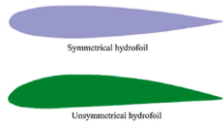
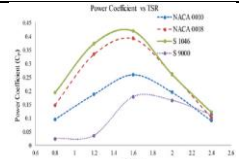
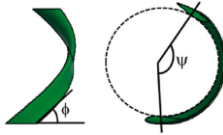
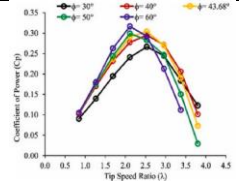
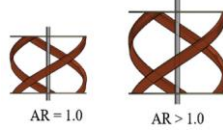
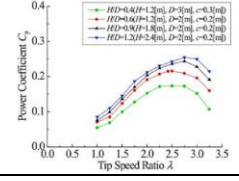
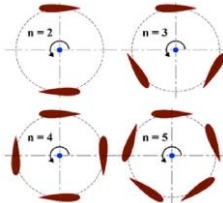
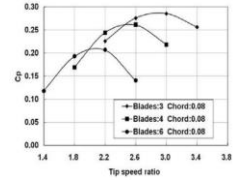
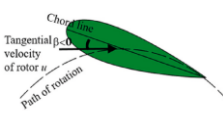
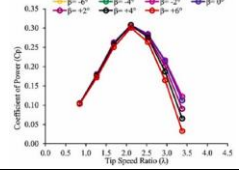
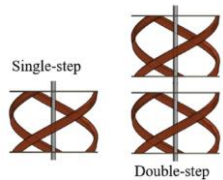
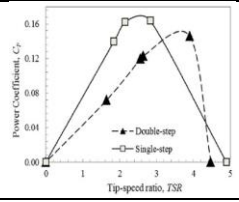
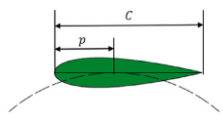
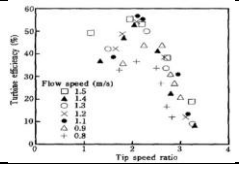
Figure 12: Schematic view of the grid for the axial hydrokinetic turbine (Niebuhr et al., 2022)

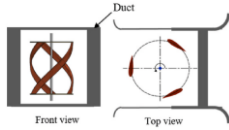
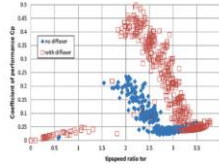
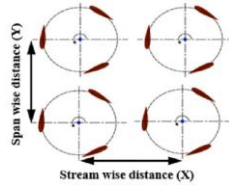
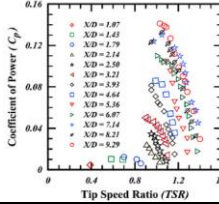
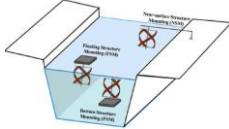
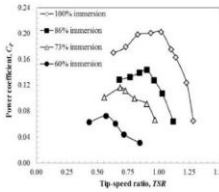
In (Wu et al., 2023), CFD techniques are used to evaluate a novel hydrokinetic turbine. The simulations model the power take-off mechanism and aim to obtain the optimized shape for the vertical turbine. The analyses have shown a significant effect of the turbine's flap angles and the inner length on the power coefficient.

Reddy et al. (2022) reviewed a couple of CFD studies to improve the efficiency of hydrokinetic turbines. These studies used geometric parameterization to analyze the power coefficient behavior based on fluid and geometric characteristics such as Reynolds number and tip speed ratio. Additionally, the researchers considered the turbine arrangements to account for the changes in performance due to device interactions. Table 2 provides a summary of the CFD studies conducted on lift-driven devices.

Table 5: Effect of various parameters on the lift-based hydrokinetic turbines (Reddy et al., 2022)

Reference	Parameter	Definition	Conceptualization	Performance Characteristic Curves
(Shiono et al., 2002)	Design parameters Solidity	Fraction of the circumference of the rotor covered by the blade $\sigma = nC/\pi D$ (Gorlov, 1995) or $\sigma = nC/D$ (Khanjanpour & Javadi, 2020).	The solidity definition illustrates that it depends on three geometric parameters: number of blades, chord length, and turbine diameter.	

Reference	Parameter	Definition	Conceptualization	Performance Characteristic Curves
(Saini & Saini, 2018)	Blade Profile	NACA hydrofoils (symmetrical/ unsymmetrical) are used to design the rotor blades.		
(R. Kumar & Sarkar, 2022)	Helicity	Blade made angle with the horizontal plane $\phi = \tan^{-1}(nH/\pi D)$ (R. Kumar & Sarkar, 2022).		
(Li et al., 2017)	Aspect Ratio	The ratio of turbine height to turbine diameter $AR = H/D$.		
(Hwang et al., 2009)	Number of Blades	The number of blades is directly proportional to the solidity.		
(R. Kumar & Sarkar, 2022)	Blade Pitch Angle	The angle between the blade chord and a tangential line is drawn to the circle of revolution of the turbine.		
(Tahukdar et al., 2017)	Number of Steps	Position of turbines one over the other.		
	Mount Point Ratio	The ratio of position of chord to chord length $MP = p/C$.		-
	Struts/ End-plates	These are used to connect the blades to the turbine shaft.	-	-
(Kihio et al., 1996)	Reynolds number	As Reynolds number (Re) increases, the torque produced by the turbine increases. $Re = (\rho v D / \mu)$.	-	

Reference	Parameter	Definition	Conceptualization	Performance Characteristic Curves
(Kirke, 2011)	Augmentation technique	This technique includes auxiliary devices such as duct/diffuser, placing foil in front of the turbine, and blocking the plate.		
(Patel et al., 2017)	Turbine arrangement	Represents the arrangement of turbines in a strategic array to avoid undesirable turbine-wake interactions.		
(Talukdar et al., 2018)	Turbine installation	The turbine can be installed in three different types of mounting schemes: bottom structure mounting, near-surface structure mounting, and floating structure mounting.		

4.5.1.5 Machine Learning Approach

Although ML has been studied to improve performance, most research has focused on the predictive maintenance of power plants and microgrid operations. This allows for the early identification of potential equipment failures, reducing downtime and increasing overall efficiency (Arafat et al., 2024). Nonetheless, this technique can improve the accuracy of failure predictions, detect and diagnose faults in real-time, and assist with the operation and maintenance of power plants. Common machine learning methodologies include Support Vector Machine (SVM), Random Forest (RF), Artificial Neural Network (ANN), Fuzzy Expert Systems (FES), and Deep Learning approaches. Critical analyses of these machine-learning methods for power plant components can be found in (Arafat et al., 2024).

Kumar et al. (2024) have devised a statistical approach to predict the efficiency of a hydro-power plant using a Kaplan turbine. Their methodology employs an Artificial Neural Network to develop models to estimate the turbine's

maximum efficiency. The neural network is implemented using 17520 samples, divided into three parts: 80% for modelling, 10% for testing, and 10% for validation. The resulting model shows an excellent fit with the data, producing a coefficient of determination (R-squared) almost equal to 1.0.

Khani et al. (2024) utilized a combination of Catboost and standalone linear regression models to predict the power coefficient, maximum power coefficient, and the corresponding tip speed ratio of a Savonius turbine in straight and bend flumes. By implementing advanced optimization techniques such as whale optimization, grey wolf optimization, and Bayesian optimization, the hybrid models achieved Savonius performance.

The research findings reveal that the combination of CastBoost and Grey Wolf Optimization integration produces the most optimal adherence among the tested methods. The study also highlights the critical role of machine learning models in identifying the sensitivity of turbine performance to inserting a returning blade deflector and the position of the current turbine

in the bend test facility. Furthermore, the study indicates that the number of turbine stages is crucial to the analysis.

In a similar investigation, Cheng et al. (2022) proposed a hybrid machine learning approach to evaluate the performance of a Dual Darrieus turbine. The prediction model involves the application of an artificial neural network, adaptive neuro-fuzzy interference system, and support vector machine to build the objective function. The optimization of the model is achieved using particle swarm optimization, simulated annealing method, and genetic algorithm. The training model incorporates an orthogonal test and computational fluid dynamics. The study demonstrates that applying hybrid machine-learning techniques yields promising results in predicting turbine performance (Cheng et al., 2022).

4.5.2 CFD modelling

This section review and report the techniques used for CFD modelling of current turbines. This includes the use of combined EFD/CFD techniques for scaling and blockage corrections and methodologies for replicating environmental conditions.

The Computational Fluid Dynamics approach has been extensively applied to study the blockage effect and wave effect on the performance of hydrokinetic turbines. The literature provides studies relating those factors to changes in power and thrust coefficients of harvesting devices. Moreover, a comprehensive wake analysis is accomplished to verify factors such as the velocity profile, the turbulence intensity, and the decay of the turbulence intensity downstream.

Schluntz & Willden (2015) analysed the effect of lateral blockage (ϵ) on a horizontal axis current turbine. They employed the blade element momentum (BEM) theory embedded into the Reynolds-Averaged Navier Stokes (RANS) solver to account for blockage ratios ranging from 0.1% to 31.4% (Figure 13). The study also examined the ratio between lateral intra-rotor spacing and the rotor diameter (s/d), which was tested between 0.25 and 100. The numerical model revealed that operating at higher blockage can lead to a more significant improvement compared to working at the turbine's design point. Therefore, the study suggests that the blockage ratio should be considered during the turbine design optimization.

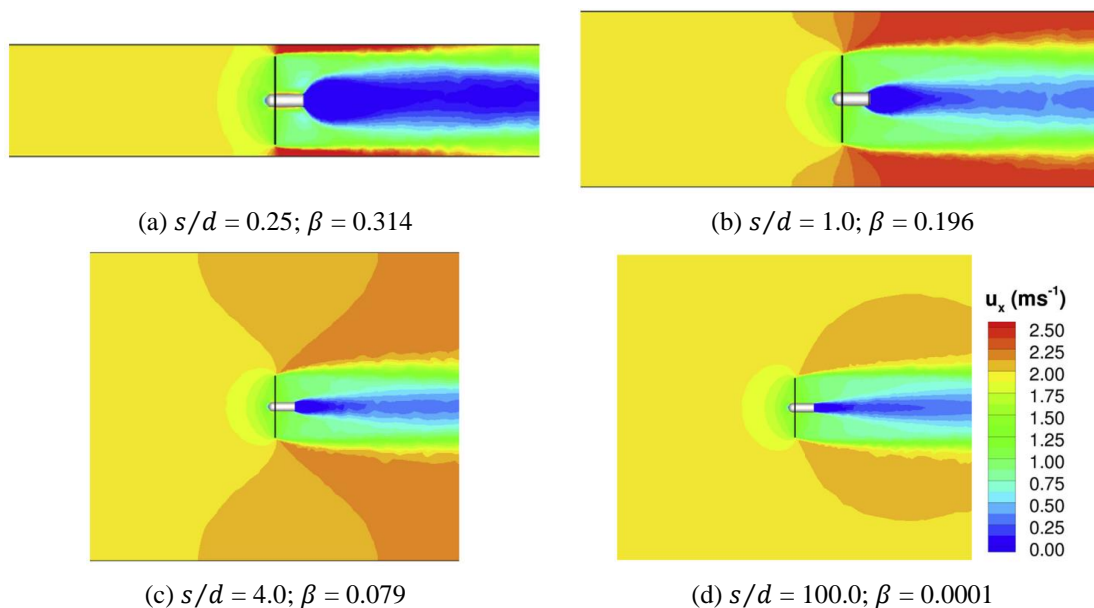


Figure 13: Ratio between the lateral intra-rotor spacing (s/d) and blockage ratio in the control volumes (Schluntz & Willden, 2015)

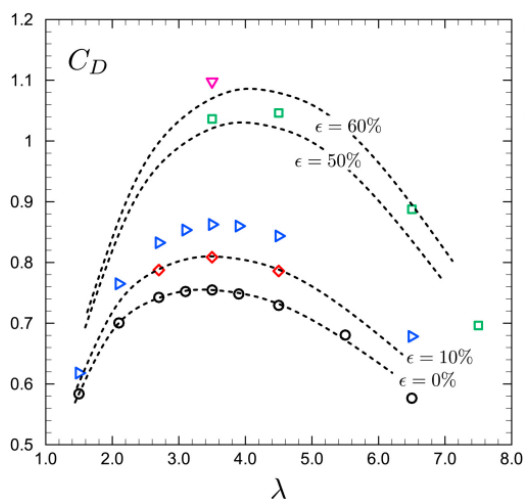
Kinsey & Dumas (2017) searched the impact of channel blockage on the performance of axial and cross-flow turbines. They employed a three-dimensional CFD model at high Reynolds numbers to achieve this. The study proposes blockage corrections for axial and cross-flow hydrokinetic turbines. These corrections enable the estimation of drag (C_D), power (C_P), and tip speed ratio (λ) for the theoretically unconfined turbine based on the results of the confined turbine. The linear momentum actuator disc theory, suitable for axial and low-solidity cross-flow turbines, was used to achieve this. Equation (1) shows the relevant details.

$$\begin{aligned} C'_P &= C_P \cdot \left(\frac{U}{U'}\right)^3 \\ C'_D &= C_D \cdot \left(\frac{U}{U'}\right)^2 \\ \lambda' &= \lambda \cdot \left(\frac{U}{U'}\right), \\ \forall \frac{U}{U'} &= \frac{\alpha_2}{\alpha_2^2 + C_D/4} \end{aligned} \quad (1)$$

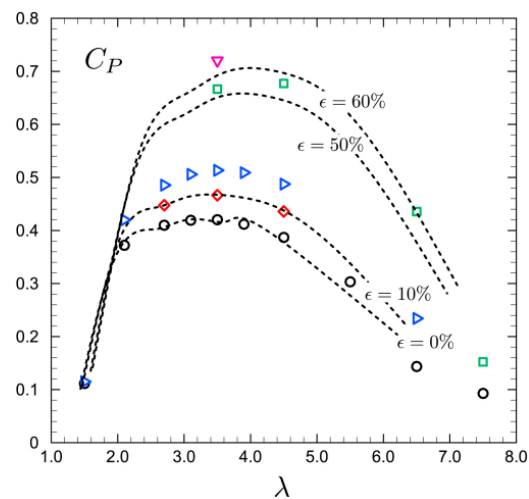
The equation above distinguishes the properties denoted by the superscript "prime" as

those belonging to an unconfined flow, while those without it refer to a confined flow. The findings indicate that the correction factor for the 3-bladed (high-solidity) cross-flow turbine is slightly underestimated by this method, especially for drag than for power. The methodology proposes the blockage correction presented in Equation (2), where the knowledge of the confined and unconfined properties enables estimating their values at another blockage condition. These adjustments are exemplified in Figure 14. Note that ϵ is another possible nomenclature for the blockage ratio.

$$\begin{aligned} C_D(\epsilon) &= \left(\frac{C_D(\epsilon_1) - C'_D}{\epsilon_1}\right) \cdot \epsilon + C'_D \\ C_P(\epsilon) &= \left(\frac{C_P(\epsilon_1) - C'_P}{\epsilon_1}\right) \cdot \epsilon + C'_P \\ \lambda(\epsilon) &= \left(\frac{\lambda(\epsilon_1) - \lambda'}{\epsilon_1}\right) \cdot \epsilon + \lambda' \end{aligned} \quad (2)$$



(a) Drag coefficient x Tip speed ratio



(b) Power coefficient x Tip speed ratio

Figure 14: Performance coefficients versus tip speed ratio (Kinsey & Dumas, 2017)

Koh and Ng (2017) studied tidal turbines using the actuator disk model and CFD simulations. They aimed to investigate the impact of various parameters on the thrust generated by the turbines. The turbines were placed in blocked conditions and exposed to a higher velocity than inflow. Results showed that the presence of boundary layers affected the thrust produced by the turbines. The turbines had less thrust when boundary layers were present in the simulation than when they were absent.

The study also revealed that an optimal aspect ratio can be achieved when boundary layers are present, leading to the maximum performance of a single turbine. This further demonstrated that the turbulence intensity and flow velocity influenced the turbine's predicted thrust. The rate of decay of turbulence intensity in the channel was found to be dependent on the channel depth, which may have affected the results.

The effect of channel depth on turbulence intensity and flow velocity can be observed in Figure 15, which compare them for experiments and turbulence models. The flow experiences a significant velocity drop (u / u_0 from 1.0 to 0.5) and a high turbulence intensity (TI = 30%) when reaching the turbine. The distance from the wake

is fundamental in determining the decay in turbulence intensity, particularly at $y / D = 1.5$, where the turbine is located. Velocity profile inflection minimizes as the downstream distance increases.

Birjandi et al. (2013) conducted a study to examine how the vertical blockage effect affects the performance of a squirrel cage turbine. The clearance coefficient, the ratio between the water height above the turbine and the turbine's diameter, is a critical parameter in this study. The clearance coefficient, denoted as C_h , can be calculated using Equation (3).

$$C_h = \frac{H}{D} \quad (3)$$

where H is the water height above the turbine and D is the turbine diameter. If C_h is negative, the water level is below the top of the rotor. Meanwhile, a positive clearance coefficient yields the water level above the turbine blades, meaning the model is submerged. The authors state this coefficient analyses the influence of both the blockage effect and free-surface effect for the power coefficient, especially in scenarios such as rivers where the water level may change throughout the year.

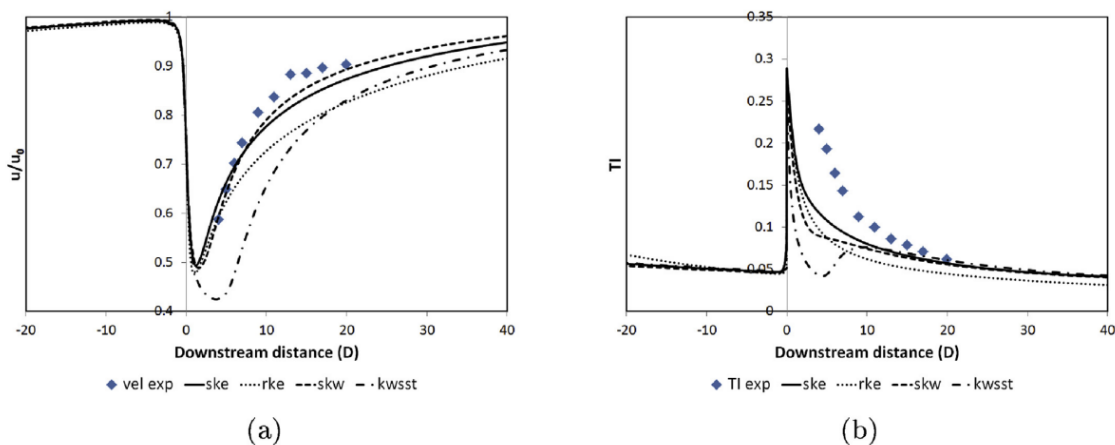


Figure 15: The a) centreline velocity and b) turbulence profiles of an actuator disk generated by the different turbulence models (Koh & Ng, 2017)

Figure 16 illustrates that the turbine performs better at slightly positive clearance coefficients. The research provides that a clearance coefficient between 0.0 and 0.2, installing the turbine a few distances from the free surface, leads to excellent performance improvement to

the device, which not only overcomes the Betz limit but also almost reaches 100% efficiency by the graph. However, negative C_h values do not allow for accessing good power coefficient values, being advised to operate in the range of 0.0 to 0.2.

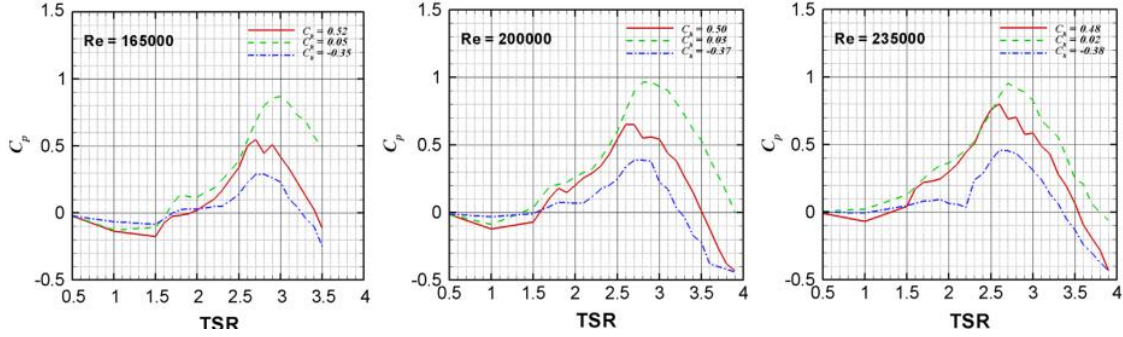


Figure 16: Power coefficient variation with clearance height at Reynolds number of (a) 165,000, (b) 200,000, and (c) 235,000 (Birjandi et al., 2013)

A study was accomplished by Kolekar & Banerjee (2015) on marine hydrokinetic turbines using numerical simulations in shallow water. The study revealed that when the turbine is positioned close to the free surface, the free-surface elevation rises, resulting in peak device performance. The device attains its highest

performance, 40%, when the clearance coefficient is 0.20 (Kolekar & Banerjee, 2015). Furthermore, Zilic de Arcos et al. (2020) studied the blockage effect for axial-flow tidal turbines and compared the results to six blockage correction methods. Table 6 Blockage correction used in (Zilic de Arcos et al., 2020) displays the various blockage corrections utilized in the study.

Table 6 Blockage correction used in (Zilic de Arcos et al., 2020)

Reference	Equation
(Glauert, 1933)	$\frac{U_T}{U_F} = \left(1 + \frac{\beta C_T}{4\sqrt{1 - C_T}} \right)^{-1} \quad (4)$
(Maskell, 1963)	$\frac{U_T}{U_F} = \sqrt{1 - \beta C_T (1 - k^2)^{-1}},$ $\forall (1 - k^2) = 0.3551 - 5.1050\beta \quad (5)$
(Pope & Harper, 1966)	$\frac{U_T}{U_F} = \frac{1}{1 + \epsilon_t}, \forall \epsilon_t = \frac{1}{4\beta} \quad (6)$
(Mikkelsen & Sørensen, 2002)	$\frac{U_T}{U_F} = \frac{1}{u + \frac{C_T}{4u}} \quad (7)$
(Bahaj et al., 2007)	$\frac{U_T}{U_F} = \frac{U_1/U_T}{(U_1/U_T)^2 + C_T/4} \quad (8)$

$$\frac{U_T}{U_F} = 1 - \beta$$

(Werle, 2010)

$$C_{T_c} = \frac{(1 - \beta)^2}{1 + \beta} C_T$$

$$C_{P_c} = (1 - \beta)^2 C_P$$

where U_T and U_F are the channel undisturbed flow velocity and the equivalent free-stream velocity, respectively. U_1 is the velocity at the turbine plane according to the actuator disc model. In Equation (7), u depends on the axial induction factor, such as $u = 1 - a$.

The Glauert method, proposed in 1933, is usually employed for aircraft propellers, assuming an equivalent free-stream velocity at equal thrust in a flume or wind tunnel. However, it only applies to thrust coefficients less than 1 ($C_T < 1.0$). The Maskell proposal, introduced in 1965, is typically used for bluff bodies but has also been used for turbines and aerodynamic profiles. For low-speed wind tunnel tests with blockage ratios between 1% and 10%, the blockage correction described by Pope & Harper in 1966 is adopted. Wind turbines are typically corrected using the method proposed by Mikkelsen & Sørensen in 2002. Bahaj et al. proposed a correction method based on the actuator disc model, while Werle's method in 2010 has been considered for correcting the measurements near the maximum extractable power.

The research indicates that the Mikkelsen & Sørensen method is most suitable for horizontal

axis turbines. The Bahaj correction can be used if the actuator disc model's induction factors are unavailable. The Maskell and Pope & Harper corrections are also recommended, but avoiding the Werle and Glauert methods for horizontal turbines is advisable.

Zhang et al. (2023) conducted tests and numerical simulations on three types of turbines - a ductless Archimedes screw hydrokinetic turbine (DAST), a Savonius turbine, and a high-solidity horizontal axis turbine - to investigate the correction methods available in the literature. Ross's bypass velocity method provided more accurate results for the DAST device. In the Savonius turbine case, Steiros's method (Steiros & Hultmark, 2018) was more suitable for corrections during operational states, while Alexander's method performed better at static states. Finally, Jeong's method was adequate for large blockage ratios, while Barnsley & Wellicome's method worked better for small blockage ratios in horizontal axis turbines.

A summary of research on blockage corrections for turbines is presented in Table 7, showing the device, the solidity ratio, the blockage ratio, and the correction factor employed in the analysis.

Table 7: Details of the correction factor in several turbines (D. Zhang et al., 2023)

Reference	Device	Solidity Ratio	Blockage Ratio	Correction Factor
(Kinsey & Dumas, 2017) ^a	Darrieus Turbine	0.25	13%, 26%, 51%	7.36%, 14.2%, 37.3%
(Kinsey & Dumas, 2017) ^a	Horizontal Axis Turbine	0.17	20%, 50%, 60%	6.9%, 17.2%, 29.6%
(Ross & Polagye, 2020b) ^a	Horizontal Axis Turbine	0.16	35%	19.1%
(Ross & Polagye, 2020b) ^a	Darrieus Turbine	0.33	36%	27.6%
(Ryi et al., 2015) ^a	Horizontal Axis Turbine	0.06	8.1%, 18%, 48.1%	1.1%, 5.9%, 12.7%
(Abutunis et al., 2021) ^a	Horizontal Axis Turbine	0.2, 0.3	19.3%	10.2%, 12.2%

(Bahaj et al., 2007) ^a	Horizontal Axis Turbine	0.07	7.5%, 17.5%	2.6%, 5.7%
(Zilic de Arcos et al., 2020) ^b	Horizontal Axis Turbine	0.06	10%, 20%, 40%	7.3%, 16%, 40.6%
(Jeon et al., 2015) ^c	Savonius Turbine	1.0	5.3%, 8.3%	6.9%, 9.5%
(Jeong et al., 2018) ^c	Darrieus Turbine	0.64	24.7%, 13.4%	9.1%, 26%
(Alexander & Holownia, 1978) ^c	Savonius Turbine	1.0	24.9%	37%
(Kinsey & Dumas, 2017) ^a	Horizontal Axis Turbine	0.17	10%, 20%, 50%, 60%	29.63%, 17.26%, 6.92%, 3.53%
(Zilic de Arcos et al., 2020) ^d	Horizontal Axis Turbine	0.06	40%	15.9%

a. Barnsley and Wellicome's method; b. Werle's method; c. Maskell's method; d. Pope and Harper's method

Note that Barnsley and Wellicome's method is an iterative method to obtain the ratio between the stream-wise velocity through the rotor (u_T) and the confined condition with the flow speed (V_0) and depends on the bypass velocity (u_b). The methodology is expressed in Figure 17. The iterative process starts with a reasonable guess of u_b / u_w . After that, it solves u_T / u_w and V_0 / u_w and checks the error between two values of V_0 / u_w . Since this value minimizes, the method converges. Otherwise, new iterations are required to achieve convergence. This method is adequate for diffuser-augmented hydrokinetic turbines (DAHT) (Du et al., 2023).

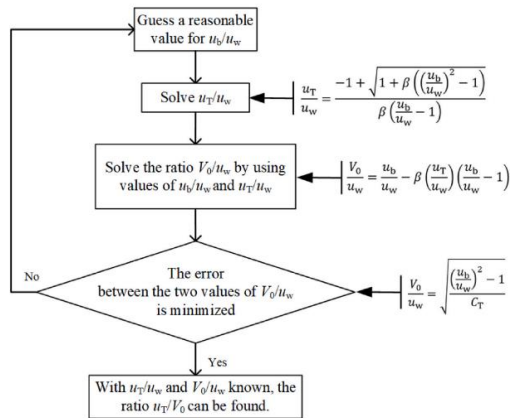


Figure 17: Flowchart of Barnsley and Wellicome's method (D. Zhang et al., 2023)

4.5.3 Modelling of arrays

Most research into turbine arrays has utilized computational fluid dynamics (CFD) techniques. These investigations examine how the

interaction between turbines in a hydrokinetic farm can impact their performance, as well as the resulting changes in the flow (such as velocity profile, turbulence intensity, and blockage effect).

Chen et al. (2021) examined the interaction between the approaching flow and tidal turbine models in a multi-row array. Porous discs were used to represent the ten horizontal axis turbines arranged in a staggered configuration with four rows. The turbines' number decreased in the streamwise direction, forming an inverted triangle layout.

According to the study, the efficiency averaged over the rows mainly depends on the velocity of the approaching flow. This is due to the blockage effect, which increases the velocity but decreases because of the wake velocity deficit. However, the additional turbines deployed six turbine diameters downstream do not exhibit a local blockage effect. Consequently, the array performance does not improve as expected in a staggered configuration. When the wakes overlap, the disadvantage of the wake shelter is reinforced, while the advantage of the blockage acceleration is lost.

The study found that the load instability becomes significant as the shear-induced turbulence intensifies, primarily among the second-row turbines. However, instability is reduced by wake overlapping. In the end, the authors imply that this configuration resulted in an efficient array performance, as expected.

Figure 18 to Figure 20 demonstrate that the turbulence intensity notably affects the second row. The row notices a turbulence intensity of about 18%. As the distance from the first row increases, the decay rate gradually decreases to reach reasonable values, such as 13%. This setup positively impacts the overall performance of the first row, as shown in Figure 21.

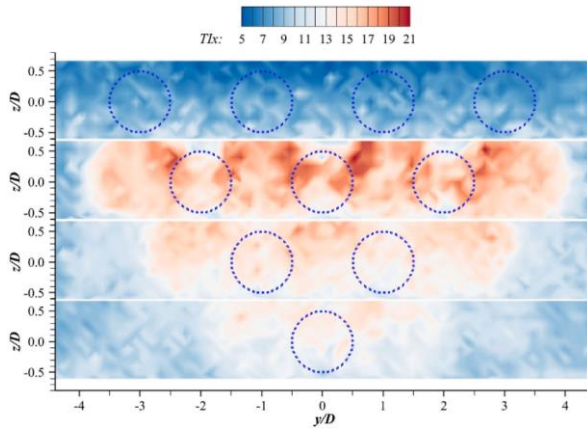


Figure 18: Streamwise turbulence intensity of approaching flow over the array cross-sections. From top to bottom, the cross-sections are located at 0D, 6D, 12D, and 18D, respectively. The blue dashed circles represent porous discs arrayed in each row (Chen et al., 2023)

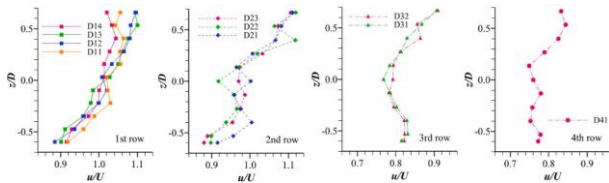


Figure 19: Vertical profiles of streamwise velocity along the vertical center axis of each disc in four rows array (Chen et al., 2023)

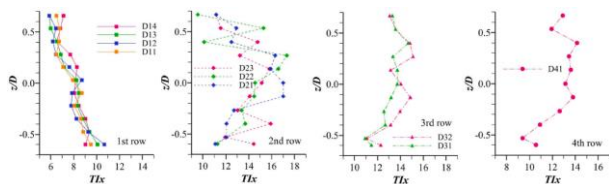


Figure 20: Vertical profiles of streamwise turbulence intensity along the vertical center axis of each disc in a rows array (Chen et al., 2023)

The data shows that the first row's thrust coefficient is significantly improved compared to a single disc with the same flow condition. With appropriate row configurations, this suggests

that there is potential for more efficient energy capture. In the first row, D12 and D13 outperform D11 and D14. When an additional row is deployed downstream, the row-averaged thrust coefficient drops from 1.08 to 1.05. This is because the staggered discs in the second row block the flow passages between neighbouring discs upstream, causing an increase in the overall resistance of the array to the oncoming flow. Consequently, more mass flow bypasses the array, reducing the first row's performance.

Djama Dirieh et al. (2022) have developed a new methodology for designing tidal farm arrays, which utilizes the actuator disk method to simulate realistic flow fields around turbine arrays. However, this method does not consider the blockage effect, which may affect the power and thrust coefficients. To address this issue, the authors have integrated an analytical blockage correction into a three-dimensional model made in Telemac3D, which modifies these coefficients. According to their findings, the blockage corrections have resulted in a 3% increase in array production over a mean spring tidal cycle. Interestingly, the power production seems to decrease when the row number in the tidal farm is increased, as shown in Figure 22.

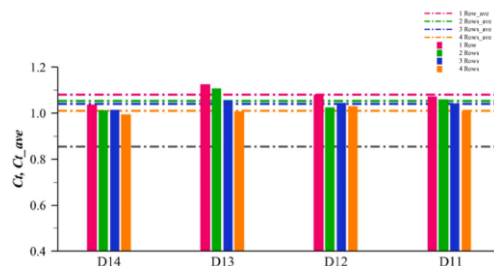


Figure 21: Thrust coefficient of each disc (bar chart) and averaged thrust coefficient of each row (dash-dotted line). The grey dash-dotted line indicates the thrust coefficient of a single disc installed in the flume. From top to bottom, the graphs show thrust coefficients for the first, second, third, and fourth rows respectively (Chen et al., 2023)

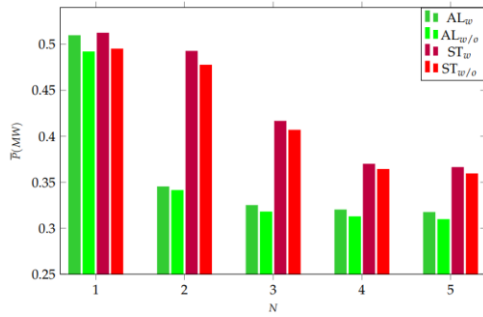


Figure 22: The mean production per row (N). For the aligned configuration, the lime green bar (AL_w) corresponds to the case with blockage correction and the green bar (AL_{w/o}) to the case without blockage correction. For the staggered configuration, the purple bar (ST_w) corresponds to the case with blockage correction, and the red bar (ST_{w/o}) to the case without blockage correction (Djama Dirieh et al., 2022)

Zhang et al. (2023) analyzed the wake interactions and performance in the twin-rotor configuration. According to their numerical analysis, the power fluctuation increases with the tip

speed ratio. A single turbine's lateral velocity deficit cloud diagram is a half-elliptical contour with the hub at its center and the tip at its initial covertices. For twin turbines, these symmetric transversal distributions are broadly exhibited. Figure 23 shows that high turbulence intensity values are computed six diameters (6D) downstream of the wake. This configuration causes symmetry in the wake, as illustrated by the graphs.

Similarly to the previous study, Soares et al. (2022) made two-dimensional simulations to estimate the efficiency of an S-shaped VAACT in a twin-rotor configuration. The results showed a 23% improvement in the turbine's performance (Soares et al., 2022a). Several new studies that model arrays of hydrokinetic turbines are presented in Table 8

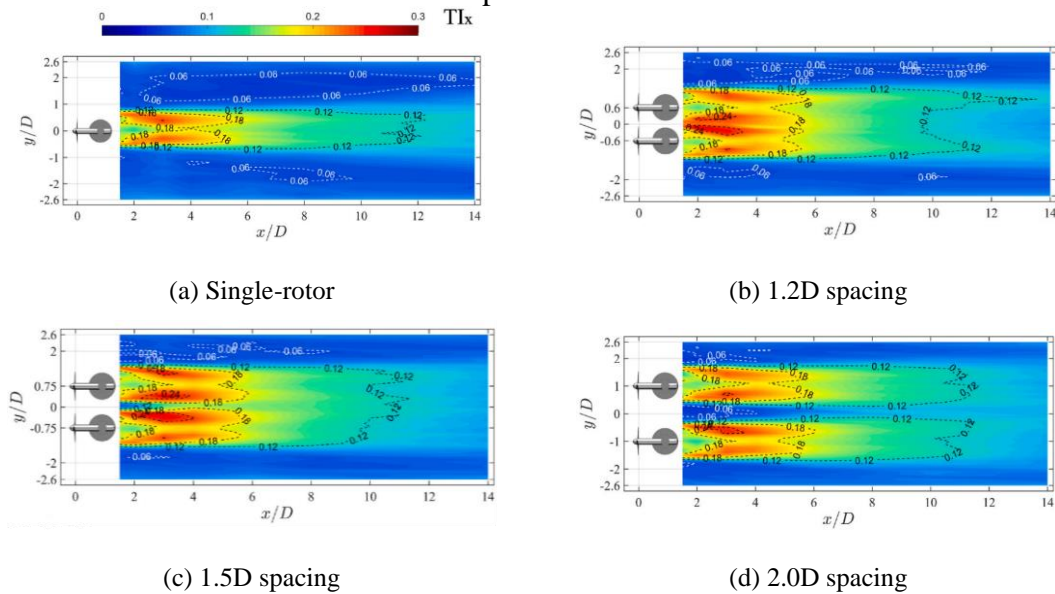


Figure 23: Horizontal wake TI_x cloud diagram (Y. Zhang et al., 2023)

Table 8: Summary of modelling arrays (Nago et al., 2022)

Type	Author	Description
River	(Guerra & Thomson, 2019)	Experiment of a crossed flow turbine of 1.5m diameter, two rotors, and flow velocity of 2 m/s upstream in the river.
Tidal and	(Nuernberg & Tao, 2018)	Experimental study of four, three-blade tidal turbine systems testing several lateral and longitudinal distances between the turbines. $V = 0.44$ m/s (velocity near to average velocity) and $D = 0.28$ m.

Type	Author	Description
Oce- anic	(Tedds, 2014)	An experiment in a channel with turbines of the horizontal axis of 3 blades, 0.5m diameter, and velocity equal to 0.9 m/s.
	(Tedds et al., 2014)	Experiment in a channel with horizontal axis turbines, 0.5m diameter, and an average velocity of 1 m/s.
	(Stallard et al., 2013)	Experiment with three blades and 0.27m diameter horizontal axis turbines. Longitudinal spacing between rows ranging from 4 to 10 D. $V = 0.47$ m/s.
	(Chawdhary et al., 2017)	A triangle diagram called Triframe is used in which a first turbine is positioned in the first row 2D away from the second row, which has two turbines. $V = 0.27$ m/s and $D = 0.15$ m. It is an experimental and CFD investigation.
	(Hill et al., 2020)	Experimental study of a dual rotor tidal turbine model. $V = 1.04$ m/s and $D = 0.5$ m.
	(Ouro et al., 2019)	Study on a tidal turbine hydrokinetic park using the Large-Scale Simulation (LES) model associated with the actuator lines model to represent the various turbines of the hydrokinetic park. Depth-averaged velocity of 0.47 m/s.
	(Mycek et al., 2014b, 2014a)	Tests to evaluate the effects of the turbulence intensity on the wakes of a tidal turbine (isolated and with two associated turbines) of 0.7 m in diameter through experimental tests with an average current velocity of 0.8 m/s.

4.5.4 Blockage corrections for testing in water channels

To address blockage issues in hydrokinetic turbines, researchers have developed studies to obtain performance curves of the turbines at various test facilities. These tests are carried out at different blockage ratios, and the results are compared to analytical formulations from existing literature. This approach helps to identify potential blockage problems and find solutions to improve the turbines' performance.

Espina-Valdés et al. (2020) performed a numerical and experimental analysis on a small

cross-flow turbine operating under high blockage effect conditions ($\beta = 45\% - 58\%$). The turbine's rotor, which measures 230 mm in chord and 300 mm in height, is connected to a timing pulley and extracts energy through a permanent magnet generator (PMG). The researchers employed an experimental setup, illustrated in Figure 24, which demonstrates that the significant blockage effect causes a deformation on the free surface, contributing to an improved turbine performance.

Analysis in Figure 25 compares the experimental and numerical results of model tests at a 306 m³/h flow rate. The numerical model doesn't account for mechanical losses, PMG performance, measurement errors, and turbulence

model inaccuracies, resulting in slight differences in the results. Despite these factors, the experimental model performs well for tip speed ratios close to 1.0 - 1.5.

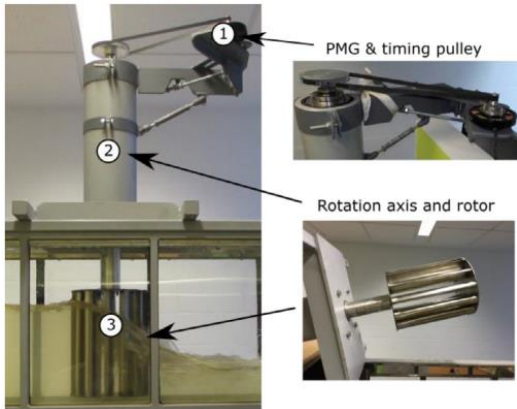


Figure 24: Experimental setup (Espina-Valdés et al., 2020)

Ross & Polagye (2020) examined blockage impact on the wake of a cross-flow turbine. The experiments were done at the University of Washington (UW). To measure the torque and forces experienced by the model test, two 6-axis load cells were placed at the top and bottom of the turbine's vertical axis. The rotational speed of the device was measured using a servo motor. Acoustic Doppler Velocimeters were installed at a gantry to capture the velocity pattern of the wake affected by the blockage effect of the test facilities in various cross-sections.

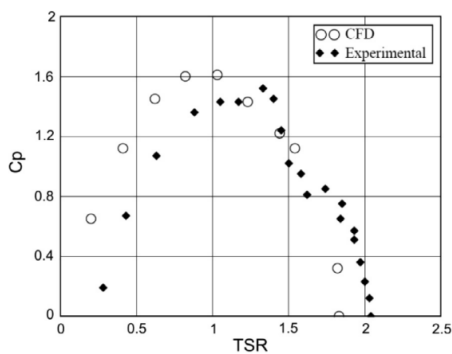
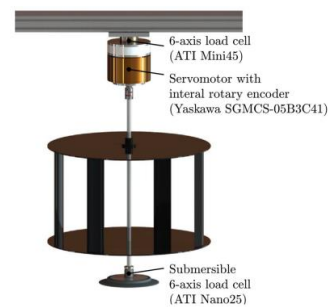


Figure 25: Power coefficient versus tip speed ratio at a flow rate of 306 m³/h (Espina-Valdés et al., 2020)

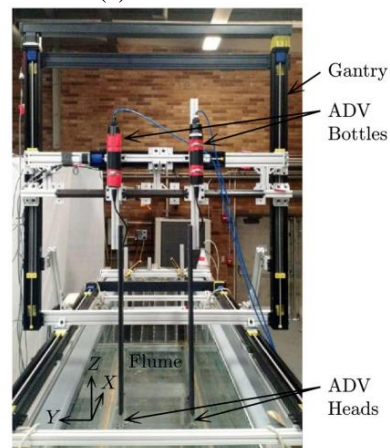
Figure 26 (a) presents the load cells, while Figure 26 (b) shows the velocity pattern. The experiments were conducted at BMSC and UW

with 14% and 36% blockage ratios, respectively. The flumes were kept at the same water depth and temperature to ensure data consistency. Additionally, the experiments were designed to have equal chord-based Reynolds numbers and depth-based Froude numbers in both cases.

Note that this study presents similarities to the analysis done by (Ross & Polagye, 2020a). The study evaluated the effectiveness of several analytical blockage corrections for cross-flow and axial-flow turbines. The investigation found that increasing blockage improved turbine performance, resulting in higher thrust and power coefficients over a broader range of tip-speed ratios. The two corrections based on measured thrust performed the best, and these corrections were more effective for the cross-flow turbine than the axial-flow turbine. The corrections performed better for thrust than power, consistent with the analytical theory's assumptions.



(a) Schematic view



(b) Test setup

Figure 26: Experimental setup for the tests performed in (Ross & Polagye, 2020b)

Figure 28 displays the wake characteristics for two blockage ratios. These characteristics include mean streamwise velocity, turbulent kinetic energy (TKE), wake extent, and viscous dissipation. The bulk structure of the wake is similar for both blockage cases, and a noticeable wake recovery is observed in the vertical direction as the core flow reduces in size at increasing X/D . The velocity of both the core and bypass flows rises as the blockage ratio increases, as the graph in Figure 28 (a) indicates.

Figure 28 (b) displays TKE, which remains relatively low near the centre and edges of the measurement region, with a sharp increase in TKE at the shear layer regardless of the blockage ratio. As we move further downstream, the shear layer becomes less defined, and the TKE near the centre and edges of the profiles rises. The analysis indicates an increase in the magnitude of TKE in the shear layer at the higher blockage ratio. Still, the magnitude of TKE outside of the shear layer remains consistent.

The wake extent is shown in Figure 28 (c). The wake contracts vertically as the core and bypass flows mix but keep a constant width. The wake is smaller for the higher blockage case at each downstream position. Still, the size difference is primarily observed in the lateral direction, and the vertical extent is relatively independent of the blockage.

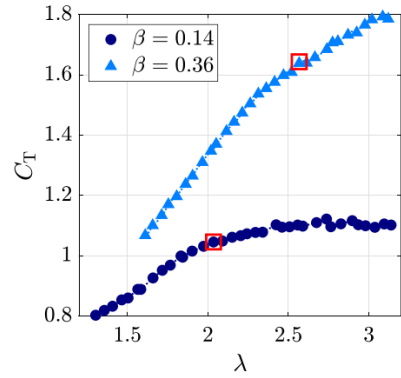
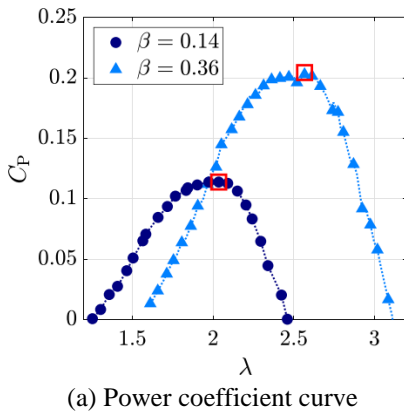
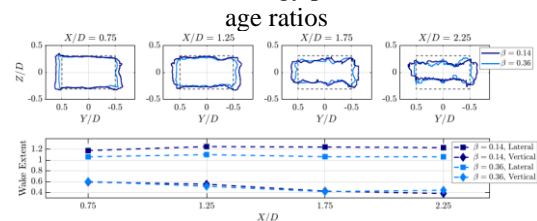
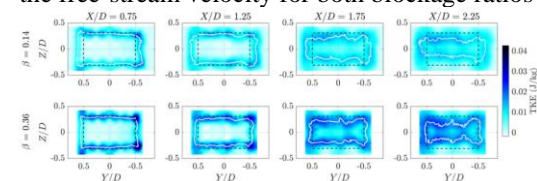
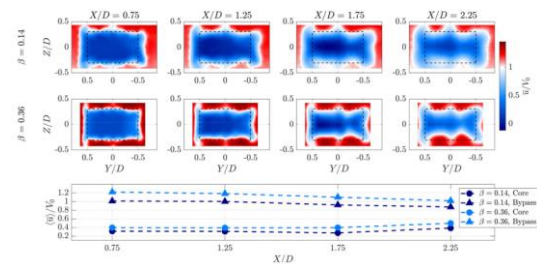
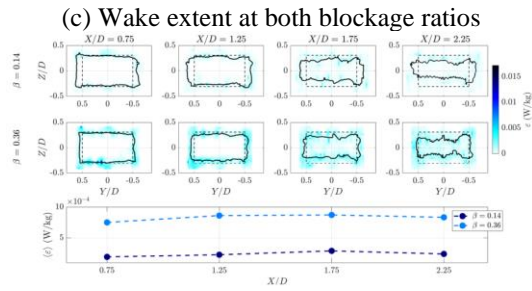


Figure 27: Results of power and thrust coefficients in the test facilities BMSC and UW (Ross & Polagye, 2020b)

Finally, Figure 28 (d) addresses the viscous dissipation rate. The dissipation rate is highest in the shear layer at $X/D = 0.75$ and $X/D = 1.25$ but is relatively uniform across the measurement region at $X/D = 1.75$ and $X/D = 2.25$. The magnitude of the dissipation rate increases with blockage. Closer to the turbine, this increase occurs primarily in the shear layer, while at further downstream positions, the dissipation rate increases throughout the measurement region. For a given blockage, the cross-sectional average dissipation rate remains relatively constant with the downstream position.





(d) Viscous dissipation rate profiles for both blockage ratios and dissipation rate averaged over each profile

Figure 28: Wake characteristics for both blockage ratios (Ross & Polagye, 2020b)

4.6 Offshore wind turbines

4.6.1 Development in model testing methodology

Reviews of the testing techniques employed for floating offshore wind turbines (FOWT) were recently published (Otter et al., 2021), (Chen et al., 2022), (Shi et al., 2023). They notably present the evolution of reproduction of aerodynamic loads on FOWTs in wave tank experiments, using either physical wind or real-time hybrid methods.

4.6.1.1 Real-Time Hybrid Model testing

Various works focusing on the real-time hybrid methods (RTHM), or software-in-the-loop (SIL), have been carried out over the last years in numerous wave tank testing facilities. These approaches have been developed in the last decade and aim at including the aerodynamic force acting on a turbine model using an actuator. This enables to overcome the difficulties in scaling down the aerodynamic loads with physical wind. The rotor is not represented with rotating blades generating aerodynamic loads, but with actuators (either cable driven robots or propellers), and the thrust can be calculated with a simple numerical model such as a drag disk model or a coupled servo-aerodynamic solver. The difficulties then lie primarily in the accuracy of the produced forces and in the speed of the real-time system.

(Bonnefoy et al., 2024) sorted existing hybrid systems for wave-tank testing according to a limited number of criteria. The following details the comparison of some of the systems presented in the recent literature, the overview is shown in Table 9.

4.6.1.1.1 Complexity of the aerodynamic model used in the real-time simulation

Some models use a simple formulation of a drag disk to represent the action of the wind on the rotor. The thrust is calculated in a very short time, with the simple use of thrust and possibly torque coefficient precomputed and stored in a look-up table, as a function of the tip speed ratio (TSR). This method is efficient, but the consideration of complex wind turbine controllers is not possible. Examples can be found in (Matoug et al., 2020), with a study on 10 MW horizontal and vertical axis wind turbines, or (Otter et al., 2022), with a study on the NREL 5 MW turbine.

Other models use a real-time servo-aerodynamic simulation of the rotor to calculate the force to be reproduced at model scale. The measured position and velocity of the physical model serve as inputs to the simulation, which can run at full scale, and the calculate force to be replicated is then Froude-scaled. A modified version of the NREL OpenFAST solver is for example used in (Azcona et al., 2019) or in (Bonnefoy et al., 2024). The simulation should be based on a simple model to be able to run in a very short time. The Blade Element Momentum is commonly used.

4.6.1.1.2 Number or components or dimensions of the reproduced force

In many studies, only the axial thrust force is being used. Consequently, the other forces induced on the rotor, e.g. aerodynamic yaw moment and gyroscopic effect, cannot be considered. This is for example the case in (Azcona et al., 2019), (Arnal, 2020), both with a propeller, and (Hall and Goupee, 2018), with a cable robot.

It is also possible to actuate a force with more than one dimension. This can include for example an asymmetrical thrust and the induced yaw moment (Ha et al, 2023). Other multi-component RTHM systems can include over two components, such as (Urbán and Guanche, 2019) that reproduces the thrust force, the rotor torque and the pitch and yaw moments, (Thys et al., 2018, Thys et al., 2021) that reproduce all force components (except for the vertical load) using a cable-driven parallel robot, or (Bonnefoy et al., 2024) that reproduce the same 5-component force using propellers.

4.6.1.1.3 The type of actuators

To date, most of the actuators make use of propellers but some use cable-driven parallel robots (Table 9). The latter makes it compulsory to implement a feedback loop to control the force applied by each winch.

4.6.1.1.4 The measurement and control of the actuated force

(Gueydon et al., 2023) emphasized the importance of the measurement of the applied force for the analysis of the measurements. (Bonnefoy et al., 2024) and (Mojallizadeh et al., 2024) present the strategy used to implement a feedback controller on a multi-component propeller-based actuator to improve the speed and accuracy of the RTHM system.

The cable-driven parallel robots are controlled with a feed-back loop, which is necessary with these systems (e.g. (Hall and Goupee, 2018), (Thys et al., 2018), (Thys et al., 2021), (Antonutti et al., 2020)), and most of the propeller-based RTHM systems use an open-loop control for more simplicity (e.g. (Urbán and Guanche, 2019), (Ha et al, 2023), (Azcona et al., 2019), (Vittori et al., 2022)), except (Bonnefoy et al., 2024) that implemented a feedback control loop as used in (Hegazy et al., 2024) to test and validate new control laws for FOWTs.

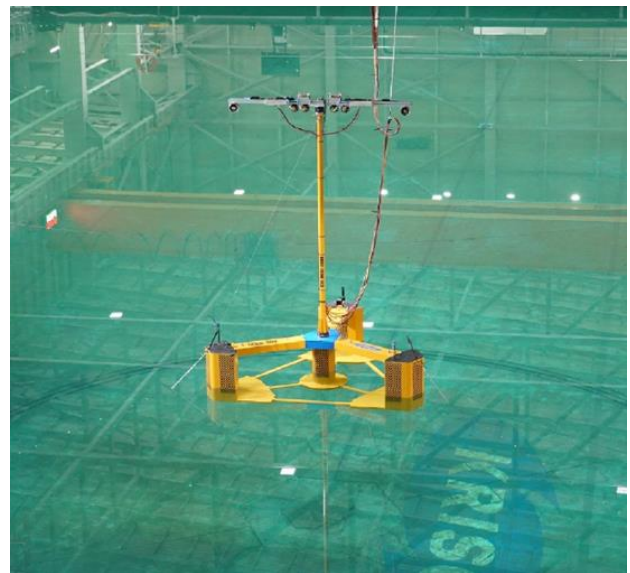


Figure 29: 10 MW class floating offshore wind turbine model with an actuator composed of ducted fans, able to reproduce thrust and yaw moments on the tower top, at the KRISO ocean engineering wave tank (Ha et al., 2023)

Table 9: Synthesis of the recent RTHM systems referenced in the literature (non-exhaustive). F_x corresponds to the axial thrust force, and F_z to the vertical force

Reference	Force calculation	Actuator	Force components						Force control
			F _x	F _y	F _z	M _x	M _y	M _z	
Hall and Goupee, 2018	RT simulation	Cables	x						Feedback
Thys et al., 2018	RT simulation	Cables	x	x		x	x	x	Feedback
Geydon et al., 2018	Look-up table	Cables	x				x	x	Feedback
Azcona et al., 2019	RT simulation	Propellers	x						open-loop
Urbán and Guanche, 2019	RT simulation	Propellers	x			x	x	x	open-loop
Arnal, 2020	RT simulation	Propellers	x						open-loop
Matoug et al., 2020	Look-up table	Propellers	x						open-loop
Antonutti et al., 2020	RT simulation	Cables	x				x	x	Feedback
Vittori et al., 2022	RT simulation	Propellers	x				x	x	open-loop
Otter et al., 2022	Look-up table	Propellers	x			x			open-loop
Ha et al., 2023	RT simulation	Propellers	x					x	open-loop
Bonnefoy et al., 2024	RT simulation	Propellers	x	x		x	x	x	Feedback

The delay can be defined as the time delay between the theoretical force that should ideally be applied at a given instant on the physical model and the force that is physically reproduced by an actuator. However, a generalized and common formulation of the force delay is still to be defined. In addition, the quantification of the total delay of the RTHM system is highly valuable in order to increase confidence in the fidelity of a RTHM system, notably for the reproduction of aerodynamic damping, which is critical for FOWTs.

The variety of developments in RTHM systems raises new questions. (Gueydon et al., 2023) points out the importance of the measurement of the force applied by the actuator. This enables a better understanding of the tests performed, identifying uncertainties and eventually a better comparison with numerical models. As pointed out in (Bonnefoy et al., 2024), a feedback controller on the applied force enables the system to reach an improved accuracy in the reproduced force (in both amplitude and delay reduction).

All actuators are limited in frequency. In most cases, they can follow the reference force on the low and wave frequency forces present in the aerodynamic force. Discrepancies arise for higher frequencies, including the 3P and the 1st

tower bending mode frequencies when it is scaled on the physical model. This is notably where the presented RTHM systems may differ.

4.6.1.2 Physical wind

The testing of FOWTs with wind physical wind and rotor blades is also being carried out in different research facilities. As presented in (Chen et al., 2022), such realization of the aerodynamic loads on scaled models can be performed using either geometrical scaled blades or performance-matched blades. In the former case, the blades dimensions are scaled using the same scaling factor as for the rest of the geometry. The Reynolds numbers occurring on the blades are then much lower than on the full-scale blades, and the induced aerodynamic effects may not be well represented. In the latter case, the blades are scaled down with a geometry that replicates closer thrust and power curves for the considered rotor.

Design procedures for these performance-matched rotors are for instance presented in (Wen et al., 2020). (Chen et al., 2018) presented a comparative study of the dynamics observed during model tests of a platform with both approaches. Mainly, the two approaches reach a good agreement, but the performance-matched

model leads to a better aerodynamic modelling than the geometry-scaled rotor (notably on the aerodynamic damping). The geometry and mass distribution however lead to differences in the gyroscopic effect, tower modes response, particularly since the 3P frequency of the geometrical-matched rotor is close to the tower eigen frequencies in the study from (Chen et al., 2018).

(Chen et al., 2022a) used a geometry-matched rotor to study the NREL 5 MW turbine supported by the OC3-Hywind spar platform at a scale 1/50. The control of the rotor was reproduced, but with a constant pitch angle for each test. The elastic properties of the tower were also captured. The analysis observed significant coupled motions between all platform rigid degrees of freedom, including a yaw response of the system. The nP harmonics in the aerodynamic force and the double frequency wave effects (second-order hydrodynamic loads) triggered the resonance of the tower bending. The latter was shown to be dominant in the resonance of the tower, highlighting the importance of high-frequency wave loads.

In (Wen et al., 2022), the analysis of the NREL 5 MW turbine supported by a spar platform with a reduced draft (50 m, full scale) was presented at scale 1/50. The spar is a redesign of the OC3-Hywind platform for moderate depth water. The blades of the rotor were geometrically scaled. The effects of the wind loads were investigated, for example by means of decay tests without wind, and with wind for a parked and rotating turbine. This shows the alteration of the surge natural frequency (mainly due to the altered mooring stiffness at a shifted position under the action of wind thrust) and damping by the aerodynamic loads. White noise wave tests were also performed without wind and with wind for an operating turbine. This exhibited that the presence of wind on the operating turbine increased the surge response, while strongly damping the pitch resonance. A significant yaw motion was also observed, probably due to the cumulated effects of imbalanced loads, mooring restoring force and gyroscopic effect as the turbine pitches.

(Madsen et al., 2020) makes the analysis of the DTU 10 MW turbine supported by a Tension Leg Platform (TLP), with a performance-matched and pitch-regulated rotor at scale 1/60. The collective blade pitch is dynamically controlled with an actuator. This experimental set-up allows the investigation of three controllers, including an open-loop controller (fixed pitch), a closed-loop controller tuned for an onshore turbine and a closed-loop controller tuned for a floating offshore wind turbine, all with collective blade pitch angle control. Their effects on the turbine dynamic response in different environmental conditions are studied. Therefore, the controllers are tuned to match the scaled thrust curve rather than the torque, as the response of the model rather than its power production is at stake in this study. The known phenomenon of negative damping with the onshore closed-loop controller was then observed during the wave tank testing, resulting in amplified motions of the turbine. The offshore controller led to a large surge displacement after shutdown, which was explained in terms of alteration of the aerodynamic damping. Amongst other conclusions, this work demonstrates that control algorithms for floating offshore wind turbines can be tested and validated with this type of experimental set-up, including Froude scaled floaters and performance-matched rotors at reduced scale.

(Yang et al., 2021) present a study on a 6 MW turbine supported by a spar platform of 76 m draft. The study considers a thrust-matched rotor. The study is made at scale 1/65.3 to match the full scale 100 m water depth in the wave tank. It focuses mostly on the low-frequency loads that would occur in an intermediate draft configuration (100 m). A comparison is made between the experimental measurements and FAST simulations. The study concludes on the importance of second order loads in the prediction of the low-frequency motions in both vertical and horizontal plane. In particular, the full QTF formulation improves the prediction of these loads and oscillations compared to Newman's

approximation. The wind and current loads can typically decrease the low natural frequencies of the system and increase the low-frequency response of the platform. They however only have little effect on the wave frequency response, where the wave loads are dominant.

(Guo et al., 2024) analyses a 12 MW rotor supported by a semi-submersible platform (tri-floater) at scale 1/70. The scaled rotor is thrust-matched, and the tower is stiffness- and geometry-matched, with a use of a light foam ring around the stiffness-matched tower. This allows a better reproduction of the aerodynamic loads on the tower. No dynamic blade pitch control was considered, but a constant blade pitch angle was set at the start of each condition. The study focuses on various environmental conditions, including waves, wind and current. It is for example highlighted that the presence of current significantly decreases the pitch motion of the turbine and the tower base loads. With strong environmental conditions, it is observed that the standard deviation of mooring loads and motions increase notably when the wind exceeds the cut-out wind speed. In operating conditions, the tower top loads are driven by the 3P effects for the shear load, and by the 1P effect for the bending moment.

4.6.1.3 Structural elasticity and internal loads (floating)

The structural elasticity and internal loads of the platform of floating wind turbine are challenging to study. Experimentally, structural similarity is possible at model scale for the tower, choosing a material (with given density and Young's modulus) and a geometry (diameter and thickness distribution) that enables to reproduce the eigen frequencies and possibly the shapes of the first structural modes. This is however difficult for the support structure because the geometry is constrained by the Froude scaling of the hydrodynamic loads on the outer shell. It is also possible to investigate internal loads on a rigid structure (as done on ships for instance), but this requires a very stiff structure, to keep all

eigen frequencies away from the frequency window of interest in the tests. For example, to investigate the vertical bending moment in the ITTC-ISSC container ship benchmark reported by (Kim and Kim, 2016), (Bouscasse et al., 2022) chose to have a natural frequency over 20 times larger than the wave frequency when $\lambda_{wave} = L_{pp}$ (λ_{wave} being the wavelength and L_{pp} the length between perpendiculars). This enabled an accurate analysis of strongly non-linear effects on the wave-structure interaction for this ship without the alteration of the measurements by the vibrations of the structure. This section presents a few studies made on elastic platforms for wind turbines.

A wind turbine supported by a lightweight semi-submersible was studied in (Suzuki et al., 2019) using an elastic model. The tower is supported by guywires for increased stiffness and mass reduction. The semi-submersible platform is composed of a central column carrying the turbine and three side columns on the side (at 120° from each other), connected with pontoons to the central column. Guywires connect the side columns to the tower top (the tension in the guywires is adjustable). The authors present a 1/80 elastically and dynamically scaled model of the turbine, scaling the bending stiffness of the pontoons. To do so, a segmented backbone (or skeleton) is designed as shown in Figure 30. The structural stiffness is scaled by the backbone and the geometry of the shell is scaled to respect the Froude scaling law. Strain gauges are mounted on the flexible beams. The model was tested in the Ocean Basin of University of San Paulo. The analysis is mostly focused on the effects of the side columns inclination and of the guy-wires tension on the dynamic response of the turbine.

Following a similar strategy, (Takata et al., 2021) designed a 1/50 scaled flexible semi-submersible tri-floater shown in Figure 31. The whole floater is made flexible thanks to an elastically scaled skeleton and geometrically scaled floaters. The skeleton (or backbone) was made of stainless steel, and the design of thin beams

enabled to down-scale the bending stiffness modulus EI , where E is the Young's modulus and I the inertia of the beam section. Strain gauges are mounted at different positions on the backbone. The study focused primarily on regular waves, showing significant elastic response of the structure, and in particular a coupling between the bending of the pontoons and the heave response. This indicates the importance of elastic effects in the design of such a platform. Comparisons with a numerical Morison based model showed a good agreement with the experimental measurements.



Figure 30: Flexible model presented in (Suzuki et al., 2019)

(Liu and Ishihara, 2021) also studied a flexible semi-submersible platform designed for a 2 MW turbine at a scale of 1/60. The flexibility of pontoons and braces is included in the model (green sections in Figure 32), where the bending stiffness modulus $K=EI$ of the elements are scaled according to Froude scaling law, meaning $K_{ms} = \frac{K_{fs}}{\lambda^5}$, where ms and fs refer to model and full scale respectively, and λ is the scaling factor.

(Leroy et al., 2022) designed a flexible spar platform supporting a wind turbine at the scale 1/40. The FOWT model was tested in the ocean engineering wave tank of Ecole Centrale de Nantes in France. The platform was composed

of a central backbone, providing a Froude-scaled 1st bending mode frequency, with light floaters mounted around to provide Froude-scaled hydrodynamic loads, as shown in Figure 33.

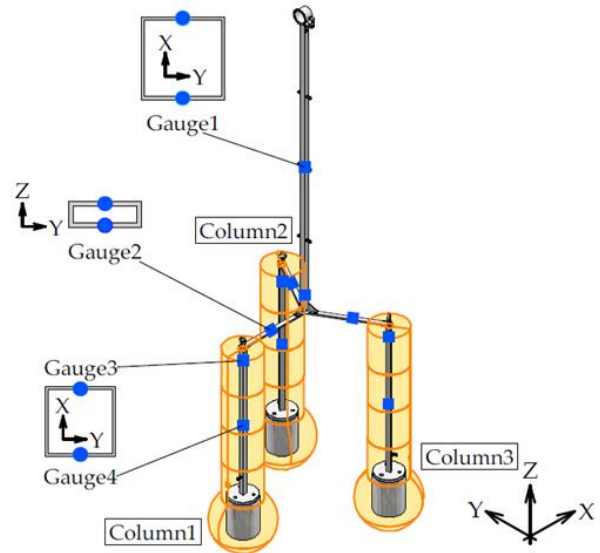


Figure 31: Flexible semi-submersible tri-floater modelled in Takata (et al. 2021)

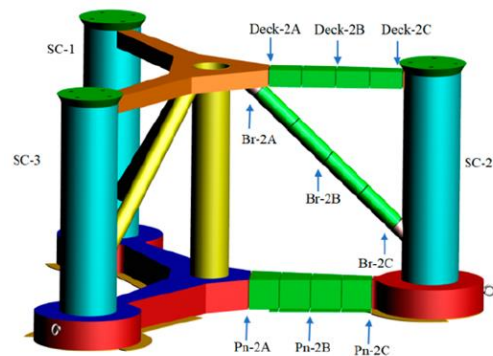


Figure 32: Flexible semi-submersible platform studied in (Liu and Ishihara, 2021)

The study includes decay tests, regular and irregular waves of various steepness. Studying the bending of the spar and its vibrations in various steep sea-states, the authors conclude on the importance of non-linear hydrodynamic loading in the emergence of resonant responses, as springing/ringing response of the structure is observed at the natural bending mode frequency. For example, Figure 34 shows the bending strain in the platform during an extreme sea-state (H_s

= 10.9 m and $T_p = 13.8$ s) at three different locations. The wave frequency response is clearly identified in the window [0.05; 0.18] Hz (at full scale), and the natural modes of surge and pitch are seen at lower frequencies. The peak at 0.38 Hz corresponds to the springing/ringing response occurring when steep wave packets reach the platform. No aerodynamic loads were considered in this study. The measurements have been published online as open-data (Leroy et al., 2024) and a comparison to low/intermediate fidelity numerical tools (based on linear potential flow and Morison equation) was also published (Ran et al., 2023).

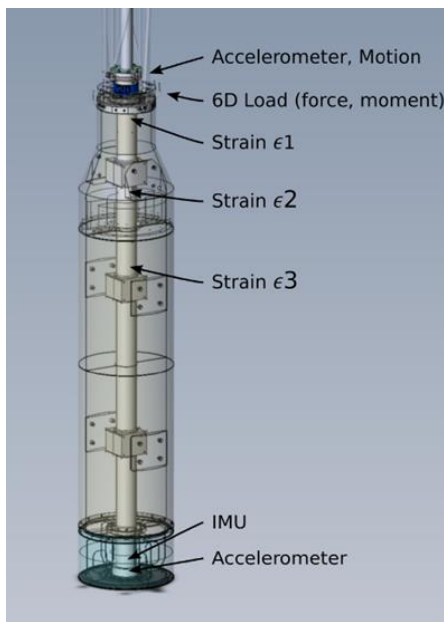


Figure 33: CAD view of the 1/40 scaled flexible spar designed and tested in (Leroy et al., 2022)

Lastly, (Hansen et al., 2024) presented an extensive analysis of high-order loads on a flexible semi-submersible platform. The model is a simplified semi-submersible presented in Figure 35. It is made of two columns, connected with a flexible pontoon beam. Two values of structural stiffness have been tested for the pontoon, leading to two different natural frequencies for the 1st flexible mode.

To the knowledge of the authors, the analysis presents a four-phase separation method applied for the first time for a floating body. This allows

a decomposition of the response of the turbine into the 0th and four first harmonics from irregular wave measurements. The inertia- and drag-driven contributions to the response can then be identified. Linear and non-linear wave-structure interaction terms can then be studied, emphasizing the importance of quadratic drag second order forcing terms in the modelling of such structure. For the soft configuration, a second-order potential flow theory based numerical model with drag was able to calculate the system's response, after calibration of the damping coefficients. Some deviation remained because of a slightly wrong estimation of the even-harmonic content of the loads. For the stiffer case, with a natural bending mode larger than the wave frequency range, the resonant response observed in the tests was not accurately, even after calibration of the damping.

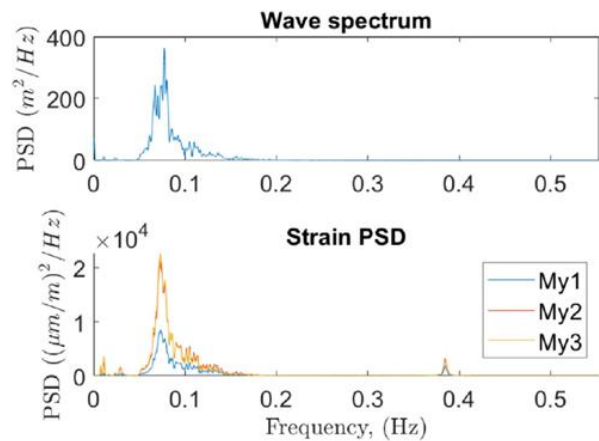


Figure 34: Bending strain power spectral density measured in the flexible platform in an extreme sea-states ($H_s = 10.9$ m and $T_p = 13.8$ s) in (Leroy et al., 2022)

The four-phase decomposition identified the forcing as third or higher harmonic in severe sea-state states. A second order based model was then unable to predict the bending resonance, even with drag. This study confirms the importance of experimental analysis on non-linear wave-structure interaction. Non-linear wave forcing terms could lead to resonant vibration outside the wave frequencies, and beyond 2nd order wave loads that can usually be included in numerical simulations.

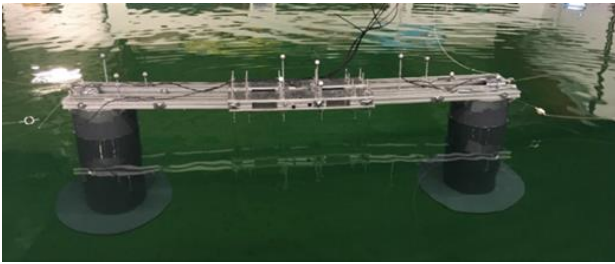


Figure 35: Simplified semi-submersible platform used in the DHI ocean tank in (Hansen et al., 2024)

4.6.2 Influence of the vertical wind profile on the operation and efficiency

The vertical wind shear profile is often modelled using a power law and a constant shear profile. However, the shape of the wind shear profile will vary, both in time and in location. The various wind profiles will influence both the power produced by the wind turbines and the loads on the wind turbine structures.

The vertical wind profile can vary for different reasons. Onshore, the different roughness in the terrain will have a great impact. However, offshore the sea is relatively smooth and the main driver for different wind shear profiles are temperature gradients. Inside the atmospheric boundary layer, the atmospheric stability is important for the shape of the vertical shear profile. The atmospheric stability is a measure of the vertical motion of air parcels. In unstable atmospheric conditions the air parcels will move upwards, while in stable atmospheric conditions these motions will be downwards. Normally one assumes that neither happens, so there is no vertical motion of the air parcels, this is neutral atmospheric conditions (Pérez Albornoz et al. 2022).

Typical wind shear profiles are shown in Figure 36. The profiles here are using the Monin-Obhukov similarity theory, which was developed for onshore but is shown to also be valid offshore (Edson and Fairall, 1998), and a log-law relationship for the vertical variations of mean wind speed (Alblas et al., 2014).

In the study by Sathe et al. (2013), wind shear for different stability conditions at 10 m/s was investigated for a 5.5 MW wind turbine at hub height 100 m. Considering the different atmospheric conditions at offshore wind sites, it was shown that it is not conservative to assume that the wind shear is always logarithmic when estimating fatigue lifetime for the blade root. Based on the findings, the largest fatigue is found for large wind shear conditions, which are often related to stable atmospheric conditions. Measurements from several offshore wind sites indicate that the stable atmospheric conditions occur often. Figure 37, taken from Alblas et al. (2014), shows the distribution of stability class at the two offshore windfarms Egmond aan Zee (OWEZ) and North Hoyle.

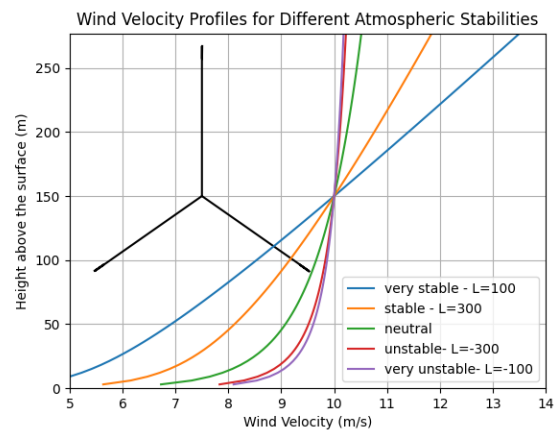


Figure 36: The vertical wind profile for different heights, considering five different stability conditions. The wind turbine in the back has the same dimensions as the IEA 15 MW, with hub height 150 m and blade length 117 m. The reference speed is 10 m/s at 150 m (hub height).

The wind shear does not have a direct impact on the power production, if one considers the wind speed at hub-height. If one considers wind speed measurements lower than hub height and extrapolate to hub height, the wind speed at hub height will depend on the wind shear and consequently the controller will behave differently depending on the wind shear (Lange et al. 2004; Motta et al. 2005).

It is important to note that the atmospheric stability also has an influence on the turbulence.

The stable conditions have typically low turbulence, while the unstable conditions have more turbulence. For a wind farm the turbulence is important for wake length. High turbulence has a shorter wake compared to the lower turbulence (Alblas et al., 2014). Figure 38 shows the

simulated wake losses at OWEZ and North Hoyle, and it is seen that the very unstable conditions with high turbulence and little vertical shear have less wake loss and higher power production.

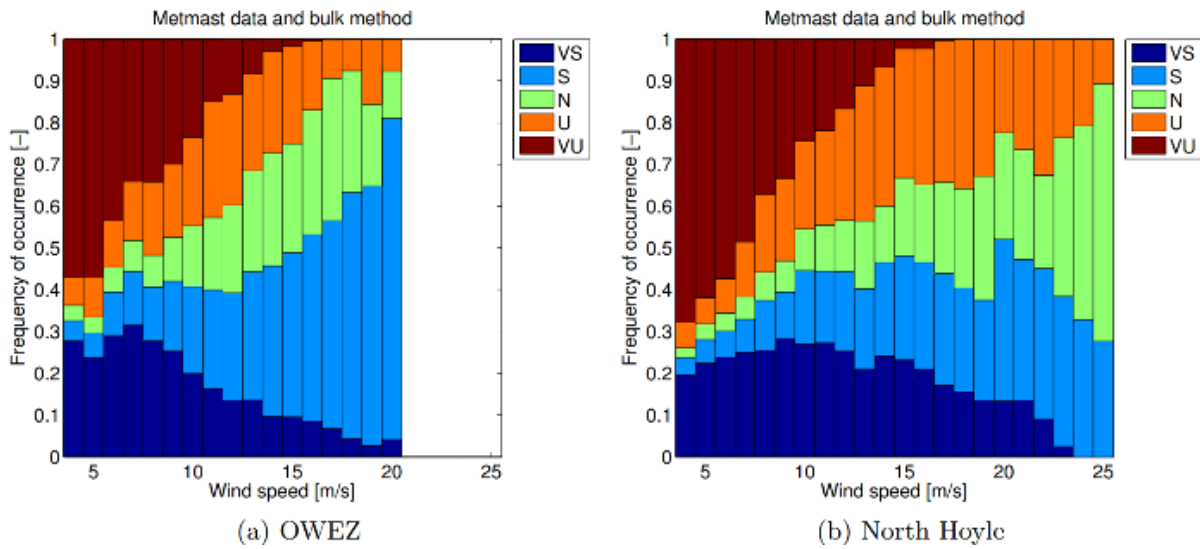


Figure 37: The distribution of stability classes versus wind speed at OWEZ and North Hoyle. VS=very stable, S=stable, N=Neutral, U=Unstable, VU=very unstable. Courtesy to Laurens Alblas, figure from Alblas et al. (2014).

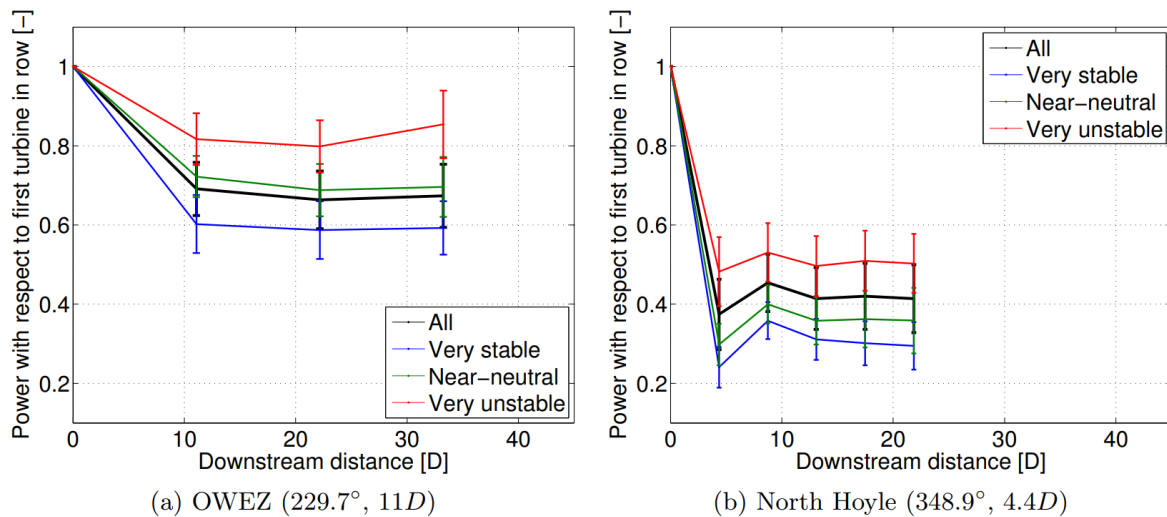


Figure 38: Simulated wake losses at (a) OWEZ and (b) North Hoyle at wind speed 8m/s. The error bars are one standard deviation. Courtesy to Laurens Alblas (Alblas et al., 2014).

Power production for wind farms is typically estimated using so-called actuator disc models. In these models the rotor is considered as a disc that extracts the energy from the incoming wind. The power produced by a wind turbine is

proportional to the cube of the inflow wind speed, the disc area and a power coefficient, C_p , representing the efficiency of the turbine in extracting power from the wind. There exist various methods on how to formulate the inflow wind speed. The traditional approach is to

consider the hub height wind speed (HHWS). However, the wind speed at hub height is not necessarily representative of the average wind speed across the rotor, especially offshore and for large wind turbines where there can be large variations in the wind profile across the rotor disc due to the atmospheric boundary layer. An alternative is to use a rotor-equivalent wind speed (REWS) model where the wind field is averaged over the area swept by the rotor blades. There are also modifications to these models that accounts for variations of wind direction, or wind veer, across the rotor disc. These methods have been applied in several studies to examine the importance of wind shear on power production, and an extensive review is given by Lopes (2021) who concluded that the choice of model will affect the estimate of power production. A few recent publications are summarized below.

Murphy et al. (2020) studied how wind speed shear and directional veer affected wind power production for a megawatt size wind turbine, employing various modelling strategies including different shear and veer metrics. Their conclusion was that REWS emerges as the most predictive metric, showcasing significant correlations with power production across a wide range of wind speeds for the specific site considered. Exploring wind power prediction at the Anholt Offshore Wind Farm in Denmark, Ryu et al. (2022) compared the effectiveness of REWS methods with the traditional HHWS method using two years of SCADA data. Results indicated that REWS tends to provide more accurate predictions than HHWS. However, this was not always consistent, likely due to variations in local atmospheric stability condition. It is therefore important to assess nearby atmospheric stability characteristics to determine whether REWS or HHWS will provide more reliable power output predictions.

The actuator disc model simplifies the representation of the rotor by treating it as a disc that extracts kinetic energy from the wind passing through it, while the BEM method divides the rotor blade into multiple elements along its length and calculates the aerodynamic forces

acting on each element. The BEM method enhance the level of complexity and details in calculating the aerodynamic performance of the wind turbine. It is generally used for aerodynamic load calculation on rotor blades in design codes, but less applied for wind power production estimates as it is more computational demanding compared to the actuator disc model.

Mata et al. (2023) examined the impact of wind speed and direction shear on wind power production by analysing LiDAR measurements alongside SCADA power measurements. The study compared HHWS and REWS with a blade element momentum (BEM) model based on their ability to account for wind shear effects. The BEM model demonstrated the highest correlation and lowest overall error with the SCADA measurements. The research highlighted the importance of accurately modelling wind shear for wind energy resource assessment and turbine design. Sensitivity analysis of the BEM model revealed its dependence on factors such as induction and turbine control. Thus, future research should include refining aerodynamic models to better account for wind shear effects and improve the tip-speed ratio estimation based on the wind conditions.

The BEM method was applied by Li et al. (2018) when they investigated the effect of wind field on the power generation and aerodynamic performance of a 5MW floating wind turbine. Three different wind fields were considered, namely a uniform wind field, a steady wind field with wind shear, and a turbulent wind field. Six different load cases were studied with wind speeds both below and above rated wind speed. All the three wind fields had the same mean wind speed at the hub height. The result from the analysis showed that the wind shear had very limited effect on the power generation and thrust force compared to a uniform wind field. But the wind shear caused noticeable effect on the local aerodynamic loads applied on the individual blades. Introduction of turbulence had also little effect on the mean power production and mean thrust force. However, the standard deviation of both power generation and thrust force increase

significantly with turbulent wind. They observed a difference in the reaction of the power generation due to low frequency turbulence depending on the operational state. This was attributed to the two different wind turbine controllers which are active in different operational states. Furthermore, the paper concluded that both fatigue and extreme loads increase with wind shear and inflow turbulence, and thus a uniform wind field is not sufficient for the analysis of the floating wind turbine behaviour.

For illustration purposes, the power production is simulated for the different shear profiles shown in Figure 36 using an aero-elastic code based on the BEM-method. A model of the IEA

15 MW (Gaertner et al. 2020) is used in the simulations.

Table 9 shows the results for the different shear profiles with a reference wind speed of 10 m/s at 150 m height. There are few differences seen in the mean values, but it is also important to consider how the loads will vary during the rotation of each blade. Figure 39 shows the blade root bending moment for different shear profiles. The very stable load case with high shear, gives a higher amplitude for the load cycle. The wind profile with the lowest shear gives a lower amplitude in the load cycle. Similar results were also found by (Sathe et al. 2013).

Table 10: Mean values of wind speed at hub, power produced, blade pitch and the out-of-plane bending of blades.
*OOP stands for Out-Of-Plane, ** FA – fore-aft.

Parameter	Very stable	Stable	Neutral	Unstable	Very stable
U_hub [m/s]	10	10	10	10	10
Power [MW]	9.9	9.7	9.6	9.7	9.7
Blade pitch [deg]	3.4	3.4	3.4	3.4	3.4
Blade root bending moment (OOP*)	32.9	32.9	32.8	33.0	33.0
Blade tip displacement (OOP*) [m]	7.4	7.4	7.4	7.4	7.4
Tower base bending moment (FA)	-104	-99.6	-95.5	-94.7	-94.6

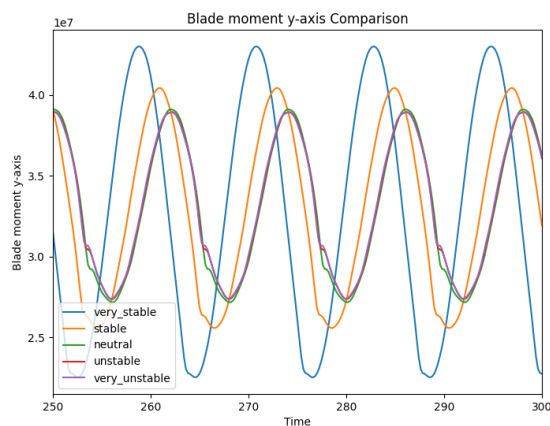


Figure 39: The blade root bending moment (OOP) with different shear profiles. The wind speed is 10 m/s at hub height for all load cases.

4.6.3 Offshore wind farm numerical modelling

Compared with onshore wind farm, floating offshore wind farm suffers more power deficit attributed by low turbulence intensity of high-quality wind resources (Xu et al, 2022). In addition, the tilting angle of FOWT will also affect the wake performance and velocity deficit (Wang et al, 2022). High-fidelity CFD simulations in combination with actuator disk or actuator line model were used, due to its computational efficiency, to reveal the underlying physical mechanism of wake interactions for floating offshore wind turbines.

Rezaeiha and Micallef (2021) utilized ANSYS Fluent in combination with an actuator disc

model to investigate the aerodynamic wake interactions of two tandem NREL 5MW FOWTs. A prescribed surge motion was imposed on the upstream rotor while the downstream one was kept fixed. They revealed that the surging motion of the upstream rotor enhanced flow mixing in the wake, which accelerates the wake recovery of the downstream rotor. These findings suggest prospects for further research on the optimization of wind farm layouts for FOWTs, to achieve more compact arrangements.

Arabgolarcheh et al. (2022) developed an actuator line model (ALM) by implementing a dedicated C++ library with OpenFOAM for exploring the near wake characteristics of FOWTs. The implemented numerical approaches are a great advantage in terms of computational efficiency compared with blade-resolving CFD methods. They revealed that the distance between two successive vortex rings and their strength undergo periodic changes in accordance with the prescribed surge motion. These variations render the intermediate wake unstable due to the mutual interaction between neighboring vortices of varying strengths.

Zhang et al. (2022) conducted a systematic analysis of the performance of significant interactions between two FOWTs by CFD based on overset mesh model. This blade-resolving

method requires approximately 32 million cell number with a small time step. They compared power output, torque and six degrees of freedom motion response under different scenarios. They revealed that tandem layout with a distance of $9.25D$ (D the rotor diameter) is the practical optimal parameter choice.

Huang, Zhao and Wan (2023) utilized an in-house CFD code FOWT-UALM-SJTU to study the coupled aero-hydrodynamic performance and wake interaction between two spar-type FOWTs with tandem and offset layouts under combined wind-wave conditions. The unsteady aerodynamic loads of the FOWT are calculated by the unsteady ALM. The dynamic responses of the FOWT, including aerodynamic loads, platform motions, and wake characteristics, are analysed in detail. Their study suggested that both platform motions and wake interaction contribute to an increased variation range of inflow wind speed experienced by the downstream FOWT, thereby increasing the instability of its aerodynamic loads. The platform motions also lead to an increase of turbulence intensity in the wake region, accelerating wake velocity recovery and widening the wake width. Figure 40 illustrates the vortex structures of the two spar-type FOWTs under different simulation conditions.

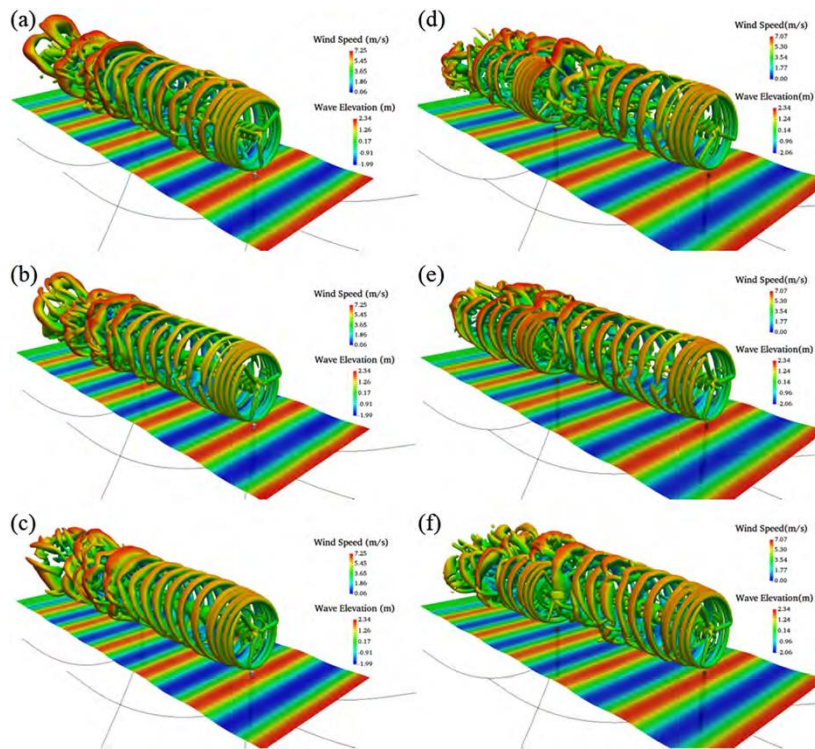


Figure 40: Vortex structures ($Q=0.002$) of two spar-type FOWTs under tandem and offset layout (Huang et al., 2023)

5. FINAL REPORT AND RECOMMENDATIONS TO THE 30TH ITTC

The 30th ITTC Specialist Committee on Ocean Renewable Energy recommends the following.

5.1.1 General recommendations

1. Continue interactions with IEC.
2. Continue the review of testing of deployment (transportation, installation) and O&M for marine renewable devices.
3. Continue reporting on full scale installation of CT, WEC, and floating OWT
4. Review of model and prototype experimental testing and numerical simulations for floating photovoltaics platforms and ocean thermal energy conversion platforms

5.1.2 Recommendations for wave energy converters (WECs)

The recommendations for future work relating to Wave Energy Converters (WECs):

1. Continue to monitor development of new concepts of WECs.
2. Continue to monitor development in PTO modelling both of physical and numerical prediction of power capture
3. Update the guidelines for numerical and experimental survival testing of WECs.
4. Update the uncertainty analysis of WEC testing include the uncertainties of the power capture and potentially of a different type of device technology.
5. Update and extend array section of guidelines for numerical modelling of WECs. (keep)
6. Review and report on the different control strategies including using AI for power optimization and survivability modes.

7. Review and report on comparisons between full scale data and numerical work/experimental model testing.

5.1.3 Recommendations for current turbines (CTs):

Some of the previous TOR could not be completed in this term due to the small number of specialists in current turbines currently assigned to the SC ORE. One key recommendation for ITTC is to assign more current turbine specialists to the SC ORE in the next term.

The recommendations for future work relating to current turbines (CTs):

1. Continue to investigate and assess data for current turbines from IEC.
2. Continue to monitor developments in physical and numerical techniques for prediction of performance of current turbines.
3. Assess support and if sufficient interest, develop specifications for a benchmark study of a horizontal axis turbine (for instance the 3-blade DoE turbine).
4. Continue review and report effects and reproduction at model scale of inflow turbulence and unsteadiness to the turbine including the effects of waves.
5. Continue review and report on the progress made on the modelling of arrays, elaborating on wake interactions and impact on performance.
6. Continue review and report blockage corrections for testing current turbines in water channels, and where necessary revise relevant guidelines and/or recommended procedures.
7. Improve procedure 7.5-02-07-03.9 Model Tests for Current Turbines, especially concerning: blockage corrections, device interference, PTO modelling, and crossflow turbines.
8. Continue monitoring the deployment of full-scale projects.

9. Review and report on methods to evaluate survivability of current turbines.

5.1.4 Recommendations for offshore wind turbines (OWTs):

The recommendations for future work relating to offshore wind turbines (OWTs):

1. Report on possible full-scale/prototype measurement data available in the public domain, assess their potential to be utilized for validation of simulation tools and evaluation of scaling effects from model scale tests.
2. Continue monitoring and reporting on the development in model testing methodology for single offshore wind turbines.
3. Review and report on model testing and numerical modelling techniques for offshore wind farms.
4. Review methodologies presented for major maintenance operations for floating wind turbines (e.g. high- and heavy lifting offshore, tow to shore, etc.).

6. CONCLUSIONS

6.1 Wave energy converters

The current level of development of large-scale wave energy generation is at a point where full-scale demonstrations are gradually beginning to take place. Commercial use of wave energy is only economically viable for off-grid applications where a small power supply is sufficient, such as the already proven light beacon buoys, or when WECs are used in multi-use coastal facilities such as breakwaters or deployed in large arrays.

In such offshore wave power farms, the interaction between WECs in close proximity (near-field effects) creates a complex wave field that affects the power extracted by each device and thus the total output of the wave power generation facility. In addition, if the farm is far

from behind the WECs (far-field effects), the farm will alter the wave field and affect coastal processes such as other users at sea, coastal ecosystems, and shorelines. Numerical and experimental modelling of arrays have each made considerable progress over the past few years, but there are still challenges. The most important advances have been the introduction of optimization techniques that allow multi-criteria selection of the location of WECs in the array, mainly in numerical calculations, and the widespread use of CFD analysis methods.

In the modelling of PTO systems for WECs, more efforts have been made in recent years to identify nonlinear effects, transient characteristics, and viscous effects. Understanding the coupling effects between PTO system components is critical to improving performance assessment, and more attention has been given to developing integrated simulation tools that can include interactions between PTO components.

However, wave energy technologies are certainly the most diverse among marine renewable energy systems. Indeed, many projects and companies have proposed unique and different ways to harness ocean wave energy. This also means that the standardization of component manufacturing and equipment with respect to wave energy is not yet organized, suggesting that the current supply chain, component manufacturing, etc., for large-scale applications is not easy to transition from one device to another. In other words, the speed of development in this area is still less than a sense of acceleration to the top TRLs. To date, none of the companies have reached a fully commercial stage, and only the Mutriku wave power plant has demonstrated stable power generation that makes commercial sense. To become more competitive, companies are gradually moving toward niche markets, off-grid applications, and integration into current or future offshore structures (breakwaters, multi-purpose platforms, harbours etc.).

Therefore, it is important to ensure thorough guidelines and procedures to assist developers through TRLs. There are still many unknowns

regarding scale effects, hydrodynamic PTO impacts, survivability testing, etc., and much of the available data is very new. As further information gradually becomes available, it will be important, if not necessary, to continually improve these guidelines and procedures.

6.2 Current turbines

The developments in current turbines today have typically been modelled using simulation through computational fluid dynamics (CFD). However, this analysis is not restricted to it. Hybrid techniques using CFD, machine learning, and semi-analytical methods support these studies for predicting current turbine performance and typical operational conditions. The experimental approach is also significant in this scenario, especially considering the analysis of small-scale current turbines, where it is worth mentioning the scale effects and uncertainty analysis. These follow the ITTC guideline 7.5-02-07-03.9 and IEC and JCGM guidelines to ensure the data repeatability and extrapolation for the full scale.

The key points in the experimental analysis consist of the limitations imposed by the test facility and the power take-off modelling. The test facility dimensions may affect the magnitude of the efficiency because of a high blockage ratio. The literature still notices the vertical blockage effect may disturb the turbine's performance. This situation has been handled through the clearance coefficient, which has a similar role to the blockage ratio.

Regarding full-scale developments, the present document has shown that the current turbine prototypes are designed to operate with flow velocity in the range 1 m/s - 3 m/s and power capacity from 1 kW to 25 kW. This suggests the developments in current turbines must achieve higher maturity levels to make the technology economically feasible. Studies have suggested that this improvement in power capacity can be achieved by optimising the turbine arrays in current/tidal farms. Nowadays, this issue is

carefully addressed because the turbulence effects of a turbine may affect other turbines downstream, decreasing their efficiency and, consequently, their power capacity.

The study of turbine layouts, especially by computational fluid dynamics, has shown that the turbine arrangement in staggered and twin rotor layouts provides promising results. According to the investigation, the turbine arrangements must be designed so that the turbulence intensity in the wake does not affect the incoming flow of the downstream turbines. Then, the challenge in modelling current turbine arrays has been to minimise the effect of the turbulence intensity at the flow and keep (or even increase) the device efficiency for the development of current turbine farms.

6.3 Offshore wind turbines

Recent studies have started to investigate experimental and numerical approaches to analyse the deployment and maintenance phases of offshore wind turbines, in addition to the traditional focus on operational and survival conditions. Experimental towing tests have observed phenomena like Vortex-Induced Motion (VIM) and analyzed towing line loads under wave conditions, numerical and experimental studies have examined the dynamic response, including heave, pitch, and roll, of semisubmersible platforms during towing, as well as bollard pull requirements, and comprehensive studies have highlighted the importance of accounting for viscous forces and non-linear effects, such as VIM, fishtailing, and pitch-induced wave run-up, in numerical models of towing operations.

In terms of full-scale floating wind turbine installations, the global offshore wind installed capacity grew from 50,623 MW in 2021 to 57.1 MW for floating projects and saw the installation of the world's largest 16 MW offshore wind turbine in China, despite challenges in fully coupled performance analysis and lightweight design for cost reduction.

Reviews of the testing techniques employed for floating offshore wind turbines (FOWT) were recently published, presenting the evolution of reproduction of aerodynamic loads on FOWTs in wave tank experiments, using either physical wind or real-time hybrid methods.

Various works focusing on the real-time hybrid methods (RTHM), or software-in-the-loop (SIL), have been carried out over the last years in numerous wave tank testing facilities. These approaches have been developed in the last decade and aim at including the aerodynamic force acting on a turbine model using an actuator. This enables to overcome the difficulties in scaling down the aerodynamic loads with physical wind. In the present report, the complexity of the correct reproduction of the aerodynamic forces, the number and dimensions of the components necessary, the type of actuators, and the measurement and control of the actuated forces have been discussed.

The testing of FOWTs with wind physical wind and rotor blades is also being carried out in different research facilities. Such realization of the aerodynamic loads on scaled models can be performed using either geometrical scaled blades or performance-matched blades. In the former case, the blades dimensions are scaled using the same scaling factor as for the rest of the geometry. The Reynolds numbers occurring on the blades are then much lower than on the full-scale blades, and the induced aerodynamic effects may not be well represented. In the latter case, the blades are scaled down with a geometry that replicates closer thrust and power curves for the considered rotor.

Due to the increasingly larger size of offshore wind turbines, and in particular floating wind turbines, it is becoming important to reproduce the flexibility of the most elongated members of the structure. Nonetheless, studying the structural elasticity and internal loads of floating wind turbine platforms is challenging. At model scale, structural similarity for the tower can be achieved by selecting materials and geometries that replicate eigenfrequencies and structural

modes. However, this is difficult for the support structure due to Froude scaling constraints on hydrodynamic loads. Investigating internal loads on a rigid structure is possible but requires an extremely stiff structure to keep eigenfrequencies outside the test frequency range. This approach is similar to methods used for ships but is complex and demanding in practice.

Modelling the vertical wind profile is important to capture its impact on the operation and efficiency of offshore wind turbines. The vertical wind shear profile, often modeled with a power law and constant shear, varies by time and location, impacting wind turbine power production and structural loads. Onshore, terrain roughness influences the profile, while offshore, temperature gradients and atmospheric stability are key factors. Atmospheric stability affects turbulence, with stable conditions leading to low turbulence and longer wakes. Traditional models use hub-height wind speed (HHWS), but rotor-equivalent wind speed (REWS) can offer more accurate predictions. Studies show that REWS better predicts power production under varying wind conditions. Accurate modeling of wind shear is crucial for turbine design and wind energy resource assessment.

In terms of wind-farm level analyses, compared with onshore wind farm, floating offshore wind farm suffers more power deficit attributed by low turbulence intensity of high-quality wind resources. In addition, the tilting angle of FOWT will also affect the wake performance and velocity deficit. High-fidelity CFD simulations in combination with actuator disk or actuator line model are used, due to its computational efficiency, to reveal the underlying physical mechanism of wake interactions for floating offshore wind turbines. However, present studies represent a wind farm with a limited number of turbines. The studies on the wake interactions of multi-FOWT wind farms are still scarce.

7. REFERENCES

- Abutunis, A., Fal, M., Fashanu, O., Chandrashekhara, K., & Duan, L. (2021). Coaxial horizontal axis hydrokinetic turbine system: Numerical modeling and performance optimization. *Journal of Renewable and Sustainable Energy*, 13(2). <https://doi.org/10.1063/5.0025492>
- Alblas, L., Bierbooms, W., Veldkamp, D., 2014, "Power Output of Offshore Wind Farms in Relation to Atmospheric Stability", *Journal of Physics: Conference Series* 555 (1): 012004, <https://doi.org/10.1088/1742-6596/555/1/012004>.
- Alexander, A. J., & Holownia, B. P. (1978). Wind tunnel tests on a savonius rotor. *Journal of Wind Engineering and Industrial Aerodynamics*, 3(4), 343–351. [https://doi.org/10.1016/0167-6105\(78\)90037-5](https://doi.org/10.1016/0167-6105(78)90037-5)
- Antonutti, R., Poirier, J. C., Gueydon, S., 2020, "Coupled testing of floating wind turbines in waves and wind using winches and software-in-the-loop", *Offshore Technology Conference*, p. D021S019R001
- Arabgolarcheh A., Jannesarahmadi S., Benini E. (2022). Modeling of near wake characteristics in floating offshore wind turbines using an actuator line method. *Renewable Energy*, 185, 871–887. <https://doi.org/10.1016/j.renene.2021.12.099>
- Arafat, M. Y., Hossain, M. J., & Alam, M. M. (2024). Machine learning scopes on microgrid predictive maintenance: Potential frameworks, challenges, and prospects. *Renewable and Sustainable Energy Reviews*, 190, 114088. <https://doi.org/10.1016/j.rser.2023.114088>
- Arnal, V., 2020 "Modélisation expérimentale d'une éolienne flottante par une approche

- "software-in-the-loop"". Ph.D. thesis. Ecole Centrale de Nantes.
- Azcona, J., Bouchotrouch, F., Vittori, F., 2019, "Low-frequency dynamics of a floating wind turbine in wave tank-scaled experiments with SIL hybrid method", *Wind Energy*, Vol. 22, No. 10, p. 1402-1413.
- Bahaj, A. S., Molland, A. F., Chaplin, J. R., & Batten, W. M. J. (2007). Power and thrust measurements of marine current turbines under various hydrodynamic flow conditions in a cavitation tunnel and a towing tank. *Renewable Energy*, 32(3), 407–426. <https://doi.org/10.1016/j.renene.2006.01.012>
- Baratchi, F., Jeans, T. L., & Gerber, A. G. (2020). Assessment of blade element actuator disk method for simulations of ducted tidal turbines. *Renewable Energy*, 154, 290–304. <https://doi.org/10.1016/j.renene.2020.02.098>
- Bastankhah, M., & Porté-Agel, F. (2014). A new analytical model for wind-turbine wakes. *Renewable Energy*, 70, 116–123. <https://doi.org/10.1016/j.renene.2014.01.002>
- Behrouzifar, A., & Darbandi, M. (2019). An improved actuator disc model for the numerical prediction of the far-wake region of a horizontal axis wind turbine and its performance. *Energy Conversion and Management*, 185, 482–495. <https://doi.org/10.1016/j.enconman.2019.02.005>
- Birjandi, A. H., Bibeau, E. L., Chatoorgoon, V., & Kumar, A. (2013). Power measurement of hydrokinetic turbines with free-surface and blockage effect. *Ocean Engineering*, 69, 9–17. <https://doi.org/10.1016/j.oceaneng.2013.05.023>
- Bonnefoy, F., Leroy, V., Mojallizadeh, M. R., Delacroix, S., Arnal, V., Gilloteaux, J.-C., 2024, "Multidimensional hybrid software-in-the-loop modeling approach for experimental analysis of a floating offshore wind turbine in wave tank experiments", *Ocean Engineering*, Vol. 309, p. 118390, <https://doi.org/10.1016/j.oceaneng.2024.118390>.
- Bouscasse, B., Merrien, A., Horel, B., De Hauteclocque, G., 2022, "Experimental analysis of wave-induced vertical bending moment in steep regular waves", *Journal of Fluids and Structures*, Vol. 111, p. 103547.
- Büttner, T.; Pérez-Collazo, C.; Abanades, J.; Hann, M.; Harper, P.; Greaves, D.; Stiesdal, H., 2022. "OrthoSpar, a novel substructure concept for floating offshore wind turbines: Physical model tests under towing conditions", *Ocean Eng.*, 245, 110508, <https://doi.org/10.1016/j.oceaneng.2021.110508>
- Chawdhary, S., Hill, C., Yang, X., Guala, M., Corren, D., Colby, J., & Sotiropoulos, F. (2017). Wake characteristics of a TriFrame of axial-flow hydrokinetic turbines. *Renewable Energy*, 109, 332–345. <https://doi.org/10.1016/j.renene.2017.03.029>
- Chen, C., Ma, Y., Fan, T., 2022, "Review of model experimental methods focusing on aerodynamic simulation of floating offshore wind turbines", *Renewable and Sustainable Energy Reviews*, Vol. 157, p. 112036.
- Chen, J., Liu, Z., Song, Y., Peng, Y., Li, J., 2022a, "Experimental study on dynamic responses of a spar-type floating offshore wind turbine", *Renewable Energy*, Vol. 196, p. 560-578
- Chen, J., Hu, Z., Wan, D., Xiao, Q., 2018, "Comparisons of the dynamical characteristics of a semi-submersible floating offshore wind turbine based on two different blade

- concepts”, *Ocean Engineering*, Vol. 153, pp. 305-318
- Chen, Y., Lin, B., & Liang, D. (2023). Interactions between approaching flow and hydrokinetic turbines in a staggered layout. *Renewable Energy*, 218, 119339. <https://doi.org/10.1016/j.renene.2023.119339>
- Cheng, B., Du, J., & Yao, Y. (2022). Machine learning methods to assist structure design and optimization of Dual Darrieus Wind Turbines. *Energy*, 244, 122643. <https://doi.org/10.1016/j.energy.2021.122643>
- Djama Dirieh, N., Thiébot, J., Guillou, S., & Guillou, N. (2022). Blockage Corrections for Tidal Turbines—Application to an Array of Turbines in the Alderney Race. *Energies*, 15(10), 3475. <https://doi.org/10.3390/en15103475>
- Du, X., Tan, J., Yuan, P., Si, X., Liu, Y., & Wang, S. (2023). Research on the blockage correction of a diffuser-augmented hydrokinetic turbine. *Ocean Engineering*, 280, 114470. <https://doi.org/10.1016/j.oceaneng.2023.114470>
- Edson, J.B., Fairall, C.W., 1998, “Similarity Relationships in the Marine Atmospheric Surface Layer for Terms in the TKE and Scalar Variance Budgets”, *Journal of the Atmospheric Sciences* 55 (13): 2311–28, [https://doi.org/10.1175/1520-0469\(1998\)055<2311:SRITMA>2.0.CO;2](https://doi.org/10.1175/1520-0469(1998)055<2311:SRITMA>2.0.CO;2).
- Elfering, K., Metoyer, R., Chatterjee, P., Mazzoleni, A., Bryant, M., & Granlund, K. (2023). Blade element momentum theory for a skewed coaxial turbine. *Ocean Engineering*, 269, 113555. <https://doi.org/10.1016/j.oceaneng.2022.113555>
- El-Shahat, S. A., Li, G., Lai, F., & Fu, L. (2020). Investigation of parameters affecting horizontal axis tidal current turbines modeling by blade element momentum theory. *Ocean Engineering*, 202, 107176. <https://doi.org/10.1016/j.oceaneng.2020.107176>
- Espina-Valdés, R., Fernández-Jiménez, A., Fernández Francos, J., Blanco Marigorta, E., & Álvarez-Álvarez, E. (2020). Small cross-flow turbine: Design and testing in high blockage conditions. *Energy Conversion and Management*, 213, 112863. <https://doi.org/10.1016/j.enconman.2020.112863>
- Fernandes, A. C., & Mirzaeifayat, S. (2015). Flow induced fluttering of a hinged vertical flat plate. *Ocean Engineering*, 95, 134–142. <https://doi.org/10.1016/j.oceaneng.2014.12.009>
- Fernandes, A. C., & Rostami, A. B. (2015). Hydrokinetic energy harvesting by an innovative vertical axis current turbine. *Renewable Energy*, 81, 694–706. <https://doi.org/10.1016/j.renene.2015.03.084>
- Gaertner, E., Rinker, J., Sethuraman, L., Zahle, F., Anderson, B., Barter, G., Abbas, N, et al., 2020, “IEA Wind TCP Task 37: Definition of the IEA 15-Megawatt Offshore Reference Wind Turbine”, NREL/TP--5000-75698, 1603478. <https://doi.org/10.2172/1603478>.
- Ghafari Hamid, R., Hassan, G., Guanghua, H., 2021, “Numerical study of the Wavestar wave energy converter with multi-point-absorber around DeepCwind semisubmersible floating platform”, *Ocean. Eng.* 232, 109177
- Giassi, M., et al., 2020, “Comparison of wave energy park layouts by experimental and numerical methods”, *J. Mar. Sci. Eng.* 8 (10) 750

- Glauert, H. (1933). Wind tunnel interference on wings, bodies and airscrews.
- Gorlov, A. M. (1995). The helical turbine: A new idea for low-head hydro.
- Guerra, M., & Thomson, J. (2019). Wake measurements from a hydrokinetic river turbine. *Renewable Energy*, 139, 483–495. <https://doi.org/10.1016/j.renene.2019.02.052>
- Gueydon, S., Lindeboom, R., van Kampen, W., de Ridder, E.-J., 2018, “Comparison of Two Wind Turbine Loading Emulation Techniques Based on Tests of a TLP-FOWT in Combined Wind, Waves and Current”, International Conference on Offshore Mechanics and Arctic Engineering, Vol. 51975, p. V001T01A012
- Gueydon, S., Bayati, I., Bosman, R., van Kampen, W., de Ridde, E.-J., 2023, “Wind Turbine Load Monitoring During Model-Test in a Wave Basin”, International Conference on Offshore Mechanics and Arctic Engineering, Vol. 86908, p. V008T09A040
- Guo, J., Liu, M., Fang, Z., Chen, W., Pan, X., Yang, L., 2024, “An experimental study on the influence of wind-wave-current coupling effect on the global performance of a 12 MW semi-submersible floating wind turbine”, *Ocean Engineering*, Vol. 304, p. 117795
- Ha, Y.-J., Ahn, H., Park, S., Park, J.-Y., Kim, K.-H., 2023, “Development of hybrid model test technique for performance evaluation of a 10 MW class floating offshore wind turbine considering asymmetrical thrust”, *Ocean Engineering*, Vol. 272, p. 113783
- Hall, M., Goupee, A.J., 2018, “Validation of a hybrid modeling approach to floating wind turbine basin testing”, *Wind Energy*, Vol. 21, pp. 391–408.
- Hansen, C. L., Bredmose, H., Vincent, M., Steffensen, S. E., Pegalajar-Jurado, A., Jensen, B., Dixen, M., 2024, “Resonant response of a flexible semi-submersible floating structure: experimental analysis and second-order modelling”, *Journal of Fluid Mechanics*, Vol 982, A7
- Hegazy, A., Naaijen, P., Leroy, V., Bonnefoy, F., Pérignon, Y., van Wingerden, J. W., 2024, “The potential of wave feedforward control for floating wind turbines: A wave tank experiment”, *Wind Energy Science Discussions*, pp. 1-30
- Hill, C., Neary, V. S., Guala, M., & Sotiropoulos, F. (2020). Performance and Wake Characterization of a Model Hydrokinetic Turbine: The Reference Model 1 (RM1) Dual Rotor Tidal Energy Converter. *Energies*, 13(19), 5145. <https://doi.org/10.3390/en13195145>
- Howland, M. F., Lele, S. K., & Dabiri, J. O. (2019). Wind farm power optimization through wake steering. *Proceedings of the National Academy of Sciences*, 116(29), 14495–14500. <https://doi.org/10.1073/pnas.1903680116>
- Huang, Y., Zhao, W., & Wan D. (2023). Wake interaction between two spar-type floating offshore wind turbines under different layouts. *Physics of Fluids*, 35, 097102. <https://doi.org/10.1063/5.0161759>
- Hwang, I. S., Lee, Y. H., & Kim, S. J. (2009). Optimization of cycloidal water turbine and the performance improvement by individual blade control. *Applied Energy*, 86(9), 1532–1540. <https://doi.org/10.1016/j.apenergy.2008.11.009>
- Hyland, T.; Adam, F.; Dahlias, F.; Großmann, J. (2014), “Towing tests with the GICON®-TLP for wind turbines. In Proceedings of the ISOPE International Ocean and Polar Engineering Conference, Busan, Republic of Korea, 15–20 June 2014.

- IEC. (2022). Marine energy - Wave, tidal and other water current converters - Part 202: Early stage development of tidal energy converters - Best practices and recommended procedures for the testing of pre-prototype scale devices.
- IEA OES, 2021, Annual Report: An Overview of Ocean Energy Activities in 2021
- IEA OES, 2022, Annual Report: An Overview of Ocean Energy Activities in 2022
- IEA OES, 2023, Annual Report: An Overview of Ocean Energy Activities in 2023
- JCGM. (2008). Evaluation of measurement data - Guide to the expression of uncertainty in measurement.
- Jeon, K. S., Jeong, J. I., Pan, J.-K., & Ryu, K.-W. (2015). Effects of end plates with various shapes and sizes on helical Savonius wind turbines. *Renewable Energy*, 79, 167–176. <https://doi.org/10.1016/j.renene.2014.11.035>
- Jeong, H., Lee, S., & Kwon, S.-D. (2018). Blockage corrections for wind tunnel tests conducted on a Darrieus wind turbine. *Journal of Wind Engineering and Industrial Aerodynamics*, 179, 229–239. <https://doi.org/10.1016/j.jweia.2018.06.002>
- Junki, F., Murai, M., Qiao, L., 2020, “Research on how the arrangement of arrayed PAWECs influences to their electric power generation”, *J. Jpn. Soc. Nav. Archit. Ocean Eng.* 31 (2020) 59–71
- Kagemoto, H. and Yue D., 1986, “Interactions among multiple three-dimensional bodies in water waves: an exact algebraic method”, *J. Fluid Mech.* 166 (1986) 189–209
- Khani, M. S., Shahsavani, Y., Mehraein, M., Soleimani Rad, M. H., & Nikbakhsh, A. A. (2024). Evaluation of the performance of the Savonius hydrokinetic turbines in the straight and curved channels using advanced machine learning methods. *Energy*, 290, 130189. <https://doi.org/10.1016/j.energy.2023.130189>
- Khanjanpour, M. H., & Javadi, A. A. (2020). Optimization of the hydrodynamic performance of a vertical Axis tidal (VAT) turbine using CFD-Taguchi approach. *Energy Conversion and Management*, 222, 113235. <https://doi.org/10.1016/j.enconman.2020.113235>
- Kiho, S., Shiono, M., & Suzuki, K. (1996). The power generation from tidal currents by darrieus turbine. *Renewable Energy*, 9(1–4), 1242–1245. [https://doi.org/10.1016/0960-1481\(96\)88501-6](https://doi.org/10.1016/0960-1481(96)88501-6)
- Kim, Y., Kim, J.H., 2016, “Benchmark study on motions and loads of a 6750-TEU container-ship”, *Ocean Engineering*, Vol 119, pp. 262–273
- Kinsey, T., & Dumas, G. (2017). Impact of channel blockage on the performance of axial and cross-flow hydrokinetic turbines. *Renewable Energy*, 103, 239–254. <https://doi.org/10.1016/j.renene.2016.11.021>
- Kirke, B. K. (2011). Tests on ducted and bare helical and straight blade Darrieus hydrokinetic turbines. *Renewable Energy*, 36(11), 3013–3022. <https://doi.org/10.1016/j.renene.2011.03.036>
- Koh, W. X. M., & Ng, E. Y. K. (2017). A CFD study on the performance of a tidal turbine under various flow and blockage conditions. *Renewable Energy*, 107, 124–137. <https://doi.org/10.1016/j.renene.2017.01.052>
- Kolekar, N., & Banerjee, A. (2015). Performance characterization and placement of a marine hydrokinetic turbine in a tidal channel under boundary proximity and blockage

- effects. *Applied Energy*, 148, 121–133. <https://doi.org/10.1016/j.apenergy.2015.03.052>
- Kulkarni, S. S., Wang, L., Golsby, N., & Lander, M. (2022). Fluid-structure interaction based optimisation in tidal turbines: A perspective review. *Journal of Ocean Engineering and Science*, 7(5), 449–461. <https://doi.org/10.1016/j.joes.2021.09.017>
- Kumar, K., Kumar, A., Saini, G., Mohammed, M. A., Shah, R., Nedoma, J., Martinek, R., & Kadry, S. (2024). Performance Monitoring of Kaplan Turbine Based Hydropower Plant under Variable Operating Conditions Using Machine Learning Approach. *Sustainable Computing: Informatics and Systems*, 100958. <https://doi.org/10.1016/j.susc-com.2024.100958>
- Kumar, R., & Sarkar, S. (2022). Effect of design parameters on the performance of helical Darrieus hydrokinetic turbines. *Renewable and Sustainable Energy Reviews*, 162, 112431. <https://doi.org/10.1016/j.rser.2022.112431>
- Konispoliatis, D.N., Katsaounis, G.M., Manolas, D.I., Soukissian, T.H., Polyzos, S., Mazarakos, T.P., Voutsinas, S.G. and Mavrakos, S.A., 2021, “REFOS: a renewable energy multi-purpose floating offshore system. *Energies*”, 14(11), p.3126. <https://doi.org/10.3390/en14113126>.
- Lange, B., Larsen, S., Højstrup, J., Barthelmie, R., 2004, “Importance of Thermal Effects and Sea Surface Roughness for Offshore Wind Resource Assessment”, *Journal of Wind Engineering and Industrial Aerodynamics* 92 (11): 959–88, <https://doi.org/10.1016/j.jweia.2004.05.005>.
- Le, C.; Ren, J.; Wang, K.; Zhang, P.; Ding, H. (2021), “Towing Performance of the Submerged Floating Offshore Wind Turbine under Different Wave Conditions”, *J. Mar. Sci. Eng.*, 9, 633, <https://doi.org/10.3390/jmse9060633>.
- Leroux, T., Osbourne, N., & Groulx, D. (2019). Numerical study into horizontal tidal turbine wake velocity deficit: Quasi-steady state and transient approaches. *Ocean Engineering*, 181, 240–251. <https://doi.org/10.1016/j.oceaneng.2019.04.019>
- Leroy, V., Delacroix, S., Merrien, A., Bachynski-Polić, E. E., Gilloteaux, J.-C. 2022, “Experimental investigation of the hydro-elastic response of a spar-type floating offshore wind turbine”, *Ocean Engineering*, Vol. 255, p. 111430
- Leroy, V., Delacroix, S., Merrien, A., Bachynski-Polić, E. E., Gilloteaux, J.-C., 2024, “Hydroelastic response of the scaled model of a floating offshore wind turbine platform in waves: HELOFOW Project Database (1.0.1) [Data set]”. Zenodo.
- Li, L., Liu, Y., Yuan, Z., Gao, Y. 2018, “Wind field effect on the power generation and aerodynamic performance of offshore float-ing wind turbines”. *Energy* 157:379–390. <https://doi.org/10.1016/j.energy.2018.05.183>.
- Li, Q., Maeda, T., Kamada, Y., Shimizu, K., Ogasawara, T., Nakai, A., & Kasuya, T. (2017). Effect of rotor aspect ratio and solidity on a straight-bladed vertical axis wind turbine in three-dimensional analysis by the panel method. *Energy*, 121, 1–9. <https://doi.org/10.1016/j.energy.2016.12.112>
- Li, Y., Yu, Y.H., 2012, “A synthesis of numerical methods for modeling wave energy converter-point absorbers”, *Renew. Sustain. Energy Rev.* 16, 4352–4364
- Liu, Y., Ishihara, T., 2021, “Numerical study on sectional loads and structural optimization of

an elastic semi-submersible floating platform”, *Energies*, Vol 14, No 1, 182

- Lopes, P.E., 2021, “Improved Wind Power Estimation Method for Operation & Maintenance of Offshore Wind Farm”, Master thesis, University of Stavanger, <https://hdl.handle.net/11250/2786258>.
- Madsen, F. J., Nielsen, T. R. L., Kim, T., Bredmose, H., Pegalajar-Jurado, A., Mikkelsen, R. F., Lomholt, A. K., Borg, M., Mirzaei, M., Shin, P., 2020, “Experimental analysis of the scaled DTU10MW TLP floating wind turbine with different control strategies”, *Renewable Energy*, Vol. 155, pp. 330-346
- Magagna, D. 2019, Ocean Energy Technology Development Report, EUR 29907 EN, Joint Research Centre of the European Commission, Luxembourg, https://publications.jrc.ec.europa.eu/repository/bitstream/JRC118296/jrc118296_1.pdf
- Mas-Soler, J.; Uzunoglu, E.; Bulian, G.; Soares, C.G.; Souto-Iglesias, A., 2021. “An experimental study on transporting a free-float capable tension leg platform for a 10 MW wind turbine in waves”, *Renew. En.*, 179, 2158–2173, <https://doi.org/10.1016/j.renene.2021.08.009>
- Manwell, J. F., McGowan, J. G., & Rogers, A. L. (2002). *Wind energy explained: theory, design and application* (E. J. W. Press, Ed.).
- Mata, S.A., Martínez, J.J.P., Quesada, J.B., Larrañaga, F.P., Yadav, N., Chawla, J.S., Howland, M.F., 2023, “Modeling the effect of wind speed and direction shear on utility-scale wind turbine power production”, arXiv:2309.15254 [physics.flu-dyn], <https://doi.org/10.48550/arXiv.2309.15254>
- Matoug, C., Augier, B., Paillard, B., Maurice, G., Sicot, C., Barre, S. 2020, “An hybrid approach for the comparison of VAWT and HAWT performances for floating offshore wind turbines”, *Journal of Physics: Conference Series*, Vol. 1618, No. 3, p. 032026.
- Mercadé Ruiz, P., Ferri, F., Kofoed, J.P., 2017, “Experimental validation of a wave energy converter array hydrodynamics tool”, *Sustainability* 9 (1) 115
- Mikkelsen, R., & Sørensen, J. N. (2002). Modelling of wind turbine blockage. 15th IEA Symposium on the Aerodynamics of Wind Turbines.
- Mirzaeifath, S., & Fernandes, A. C. (2013). Stability analysis of the fluttering and auto-rotation of flow-induced rotation of a hinged flat plate. *Journal of Hydrodynamics*, 25(5), 755–762. [https://doi.org/10.1016/S1001-6058\(13\)60422-9](https://doi.org/10.1016/S1001-6058(13)60422-9)
- Motta, M., Barthelmie, R. J., Vølund, P., 2005. “The Influence of Non-Logarithmic Wind Speed Profiles on Potential Power Output at Danish Offshore Sites”, *Wind Energy* 8 (2): 219–36, <https://doi.org/10.1002/we.146>.
- Mojallizadeh, M. R., Bonnefoy, F., Ohana, J., Delacroix, S., Leroy, V., Bouscasse, B., Weber, M., 2024, “Control design for thrust generators with application to wind turbine wave-tank testing: a sliding-mode control approach with Euler backward time-discretization”, *Control Engineering Practice*, Vol. 146, p. 105894
- Murai, M., Qiao, L., Junki, F., 2019, “Study on the generated power changes by the relation between an arrangement of an array of point absorber type WECs and an incident wave angle”, *Proceeding International Conference on Offshore Mechanics and Arctic Engineering*, vol. 58882, American Society of Mechanical Engineers, Glasgow, Scotland, UK, pp. 9–14
- Murai, M., Junki, F., Qiao, L., 2020, “How the hydrodynamic response of PA-WECs’ array, under maximizing the power generation by its arrangement and control force change?”,

- in: Proceeding International Conference on Offshore Mechanics and Arctic Engineering, vol. 84362 American Society of Mechanical Engineers, Virtual, Online, pp. 3–7, <https://doi.org/10.1115/omae2020-18189>.
August
- Murai, M., Qiao, L., Junki, F., 2021, “Study on power generation of single point absorber wave energy converters (PA-WECs) and arrays of PA-WECs”, *Renew. Energy* 164, 1121–1132
- Murai, M. and Sakamoto, S., 2022, “A Fundamental Study on the Potential of AI Prediction in Control Force Estimation to Maximize Power Generation of PA-WECs in Irregular Waves”, *J.JASANA OE*, Vol.35, pp.55-64
- Murphy, P., Lundquist, J.K., Fleming, P., 2020, “How wind speed shear and directional veer affect the power production of a megawatt-scale operational wind turbine”, *Win Energ. Sci.*, 5, 1169–1190, <https://doi.org/10.5194/wes-5-1169-2020>.
- Mycek, P., Gaurier, B., Germain, G., Pinon, G., & Rivoalen, E. (2014a). Experimental study of the turbulence intensity effects on marine current turbines behaviour. Part I: One single turbine. *Renewable Energy*, 66, 729–746. <https://doi.org/10.1016/j.renene.2013.12.036>
- Mycek, P., Gaurier, B., Germain, G., Pinon, G., & Rivoalen, E. (2014b). Experimental study of the turbulence intensity effects on marine current turbines behaviour. Part II: Two interacting turbines. *Renewable Energy*, 68, 876–892. <https://doi.org/10.1016/j.renene.2013.12.048>
- Nago, V. G., Santos, I. F. S. dos, Gbedjinou, M. J., Mensah, J. H. R., Tiago Filho, G. L., Camacho, R. G. R., & Barros, R. M. (2022). A literature review on wake dissipation length of hydrokinetic turbines as a guide for turbine array configuration. *Ocean Engineering*, 259, 111863. <https://doi.org/10.1016/j.oceaneng.2022.111863>
- Niebuhr, C. M., Schmidt, S., van Dijk, M., Smith, L., & Neary, V. S. (2022). A review of commercial numerical modelling approaches for axial hydrokinetic turbine wake analysis in channel flow. *Renewable and Sustainable Energy Reviews*, 158, 112151. <https://doi.org/10.1016/j.rser.2022.112151>
- Niebuhr, C. M., van Dijk, M., Neary, V. S., & Bhagwan, J. N. (2019). A review of hydrokinetic turbines and enhancement techniques for canal installations: Technology, applicability and potential. *Renewable and Sustainable Energy Reviews*, 113, 109240. <https://doi.org/10.1016/j.rser.2019.06.047>
- Nuernberg, M., & Tao, L. (2018). Experimental study of wake characteristics in tidal turbine arrays. *Renewable Energy*, 127, 168–181. <https://doi.org/10.1016/j.renene.2018.04.053>
- Ohana J., Horel B., Merrien A., Arnal V., Bonnefoy F., Brizzi G., Bouscasse B., 2022, Dataset: Wave tank testing of a multi-purpose platform with aquaculture, wind turbine and wave energy converters, <https://doi.org/10.17882/88376>.
- Ohana J., Horel B., Merrien A., Arnal V., Bonnefoy F., Brizzi G., Bouscasse B., Ruzzo C., (2023), “Wave Tank Testing of a Multi-Purpose Floating Platform with Aquaculture, Wind Turbine and Wave Energy Converters”, (2023) SSRN, <http://dx.doi.org/10.2139/ssrn.4437075>.
- Otter, A., Desmond, C., Flannery, B., Murphy, J., 2022, “Combined current and wind simulation for floating offshore wind turbines”, *Journal of Physics: Conference Series*, Vol. 2362, p. 012028.

- Otter, A., Murphy, J., Pakrashi, V., Robertson, A., Desmond, C., 2021, “A review of modelling techniques for floating offshore wind turbines”, *Wind Energy*, Vol. 25, No. 5, pp. 831–857.
- Ouro, P., Ramírez, L., & Harrold, M. (2019). Analysis of array spacing on tidal stream turbine farm performance using Large-Eddy Simulation. *Journal of Fluids and Structures*, 91, 102732. <https://doi.org/10.1016/j.jfluiddstructs.2019.102732>
- Patel, V., Eldho, T. I., & Prabhu, S. V. (2017). Experimental investigations on Darrieus straight blade turbine for tidal current application and parametric optimization for hydro farm arrangement. *International Journal of Marine Energy*, 17, 110–135. <https://doi.org/10.1016/j.ijome.2017.01.007>
- Pérez Albornoz, C., Escalante Soberanis, M.A., Ramírez Rivera, V., and Rivero, M., 2022, “Review of Atmospheric Stability Estimations for Wind Power Applications”, *Renewable and Sustainable Energy Reviews* 163 (July): 112505, <https://doi.org/10.1016/j.rser.2022.112505>
- Pope, A., & Harper, J. (1966). *Low-speed wind tunnel testing*. Wiley.
- Qiao, L., Murai, M., Kuwada, S., 2018, “A study on electrical power for multiple linear wave energy converter considering the interaction effect”, *Energies* 11 (11), 1–20, <https://doi.org/10.3390/en11112964>
- Ramachandran, R.C., Serraris, J.J., Montfort, J.H., De Ridder, E.J., Desmond, C. and Murphy, J. (2024). Towing Analysis and Validation of a Fully Assembled Floating Offshore Wind Turbine Based on an Experimental Study. *Journal of Marine Science and Engineering*, 12(4), p.689. <https://doi.org/10.3390/jmse12040689>
- Reddy, K. B., Bhosale, A. C., & Saini, R. P. (2022). Performance parameters of lift-based vertical axis hydrokinetic turbines - A review. *Ocean Engineering*, 266, 113089. <https://doi.org/10.1016/j.oceaneng.2022.113089>
- Rezaeiha, A., Micallef, D., 2021, “Wake interactions of two tandem floating offshore wind turbines: CFD analysis using actuator disc model”, *Renewable Energy*, Vol 179, pp 859–876.
- Robert, M., Dezhi, N., Boyin, D., et al. 2022, “Wave energy converter systems-status and perspectives”, in: D. Ning, B. Ding (Eds.), *Modelling and Optimization of Wave Energy Converters*, first ed., CRC Press, Boca Raton, pp.1-58, <https://doi.org/10.1201/9781003198956>
- Ross, H., & Polagye, B. (2020a). An experimental assessment of analytical blockage corrections for turbines. *Renewable Energy*, 152, 1328–1341. <https://doi.org/10.1016/j.renene.2020.01.135>
- Ross, H., & Polagye, B. (2020b). An experimental evaluation of blockage effects on the wake of a cross-flow current turbine. *Journal of Ocean Engineering and Marine Energy*, 6(3), 263–275. <https://doi.org/10.1007/s40722-020-00172-w>
- Rostami, A. B., & Fernandes, A. C. (2015). The effect of inertia and flap on autorotation applied for hydrokinetic energy harvesting. *Applied Energy*, 143, 312–323. <https://doi.org/10.1016/j.apenergy.2015.01.051>
- Rostami, A. B., & Fernandes, A. C. (2017). From fluttering to autorotation bifurcation of a flat plate in a current. *Journal of the Brazilian Society of Mechanical Sciences and Engineering*, 39(11), 4769–4784. <https://doi.org/10.1007/s40430-017-0912-8>

- Ruzzo, C., Muggiasca, S., Malara, G., Taruffi, F., Belloli, M., Collu, M., Li, L., Brizzi, G. and Arena, F., (2021), “Scaling strategies for multi-purpose floating structures physical modeling: state of art and new perspectives”, *Applied Ocean Research*, 108, p.102487, <https://doi.org/10.1016/j.apor.2020.102487>.
- Ruzzo, C., Fiamma, V., Scialò, A., Arena, F., Santoro, A., Muggiasca, S., Taruffi, F., Di Carlo, S., Larrea, I., Corvaglia, P.A. and Zuccarino, A., 2022, “Field experimental campaign on a multi-purpose floating structure: Set-up description. Trends in Renewable Energies Offshore”, pp.817-825.
- Ryi, J., Rhee, W., Chang Hwang, U., & Choi, J.-S. (2015). Blockage effect correction for a scaled wind turbine rotor by using wind tunnel test data. *Renewable Energy*, 79, 227–235.
<https://doi.org/10.1016/j.renene.2014.11.057>
- Ryu, G.H., Kim, D., Kim, D.-Y., Kim, Y.-G., Kwak, S.J., Choi, M.S., Jeon, W., Kim, B.-S., Moon, C.-J., 2022, “Analysis of vertical wind shear effects on offshore wind energy prediction accuracy applying rotor equivalent wind speed and the relationship with atmospheric stability”, *Appl. Sci.* 12, 6949, <https://doi.org/10.3390/app12146949>
- Sarmiento, J., Iturrioz, A., Ayllón, V., Guanche, R. and Losada, I.J., 2019, “Experimental modelling of a multi-use floating platform for wave and wind energy harvesting”, *Ocean Engineering*, 173, pp.761-773. <https://doi.org/10.1016/j.oceaneng.2018.12.046>
- Saini, G., & Saini, R. P. (2018). Numerical Investigation of the Effect of Blade Profile of a Darrieus Hydrokinetic Turbine. 2018 5th IEEE Uttar Pradesh Section International Conference on Electrical, Electronics and Computer Engineering (UPCON), 1–6. <https://doi.org/10.1109/UPCON.2018.8597073>
- Sathe, A., Mann, J., Barlas, T., Bierbooms, W.A.A.M., van Bussel, G.J.W., 2013, “Influence of Atmospheric Stability on Wind Turbine Loads”, *Wind Energy* 16 (7): 1013–32, <https://doi.org/10.1002/we.1528>
- Schluntz, J., & Willden, R. H. J. (2015). The effect of blockage on tidal turbine rotor design and performance. *Renewable Energy*, 81, 432–441.
<https://doi.org/10.1016/j.renene.2015.02.050>
- Shi, W., Fu, J., Ren, Z., Jiang, Z., Wang, T., Cui, L., Li, Xin, 2023, “Real-time hybrid model tests of floating offshore wind turbines: Status, challenges, and future trends”, *Applied Ocean Research*, Vol. 141, p. 103796.
- Shiono, M., Suzuki, K., & Kiho, S. (2002). Output Characteristics of Darrieus Water Turbine with Helical Blades for Tidal Current Generations. *Proceedings of the International Offshore and Polar Engineering Conference*, 859–864.
- Soares, R. B., Fernandes, A. C., & Sales Junior, J. S. (2022a). Performance Improvement of Vertical Axis Autorotation Current Turbine through Twin-Rotors. 5th International Conference on Renewable Energies Offshore, Lisbon, Portugal
- Soares, R. B., Fernandes, A. C., & Sales Junior, J. S. (2022b). Stability Analysis of Fluttering to Autorotation to Flat Plate Turbine. 5th International Conference on Renewable Energies Offshore
- Stallard, T., Collings, R., Feng, T., & Whelan, J. (2013). Interactions between tidal turbine wakes: experimental study of a group of three-bladed rotors. *Philosophical Transactions of the Royal Society A: Mathematical, Physical and Engineering Sciences*, 371(1985), 20120159. <https://doi.org/10.1098/rsta.2012.0159>

- Steiros, K., & Hultmark, M. (2018). Drag on flat plates of arbitrary porosity. *Journal of Fluid Mechanics*, 853, R3. <https://doi.org/10.1017/jfm.2018.621>
- Stratigaki, V., et al., 2014, “Wave basin experiments with large wave energy converter arrays to study interactions between the converters and effects on other users in the sea and the coastal area”, *Energies* 7 (2) 701–734
- Sun, K., Yi, Y., Zheng, X., et al. 2021, “Experimental investigation of semi-submersible platform combined with point-absorber array”, *Energy Convers. Manag.* 245, 114623
- Suzuki, H., Xiong, J., Do Carmo, L. H. S., Vieira, D. P., De Mello, P. C., Malta, E. B., Simos, A. N., Hirabayashi, S., Gonçalves, R. T., 2019 “Elastic response of a light-weight floating support structure of FOWT with guywire supported tower”, *Journal of Marine Science and Technology*, Vol 24, pp 1015-1028.
- Takata, T., Takaoka, M., Gonçalves, R. T., Houtani, H., Yoshimura, Y., Hara, K., Oh, S., Dotta, R., Malta, E. B., Iijima, K., Suzuki, H., 2021, “Dynamic behavior of a flexible multi-column FOWT in regular waves”, *Journal of Marine Science and Engineering*, Vol. 9, No. 2, 124
- Talukdar, P. K., Kulkarni, V., Das, A. K., Dwivedy, S. K., Kakoty, S. K., Mahanta, P., & Saha, U. K. (2017, December 7). In-Situ Experiments to Estimate the Performance Characteristics of a Double-Step Helical-Bladed Hydrokinetic Turbine. Volume 2. <https://doi.org/10.1115/GTINDIA2017-4572>
- Talukdar, P. K., Kulkarni, V., & Saha, U. K. (2018). Field-testing of model helical-bladed hydrokinetic turbines for small-scale power generation. *Renewable Energy*, 127, 158–167. <https://doi.org/10.1016/j.renene.2018.04.052>
- Tedds, S. C. (2014). Scale model testing of tidal stream turbines: wake characterisation in realistic flow conditions. University of Liverpool
- Tedds, S. C., Owen, I., & Poole, R. J. (2014). Near-wake characteristics of a model horizontal axis tidal stream turbine. *Renewable Energy*, 63, 222–235. <https://doi.org/10.1016/j.renene.2013.09.011>
- Thys, M., Chabaud, V., Sauder, T., Eliassen, L., Sæther, L. O., Magnussen, Ø. B., 2018, “Real-time hybrid model testing of a semi-submersible 10MW floating wind turbine and advances in the test method”, *International Conference on Offshore Mechanics and Arctic Engineering*, Vol. 51975, p. V001T01A013
- Thys, M., Souza, C., Sauder, T., Fonseca, N., Berthelsen, P.A., Engebretsen, E., Haslum, H., 2021, “Experimental investigation of the coupling between aero- and hydrodynamical loads on a 12 mw semi-submersible floating wind turbine”, *Proceedings of the ASME 2021 40th International Conference on Ocean, Offshore and Arctic Engineering*. Volume 9: Ocean Renewable Energy. Virtual, Online. June 21–30, 2021. <https://doi.org/10.1115/OMAE2021-62980>
- Urbán, A. M., Guanche, R., 2019, “Wind turbine aerodynamics scale-modeling for floating offshore wind platform testing”, *Journal of Wind Engineering and Industrial Aerodynamics*, Vol. 186, pp. 49-57
- Vittori, F., Azcona, J., Eguinoa, I., Pires, O., Rodríguez, A., Morató, Á., Garrido, C., Desmond, C., 2022, “Model tests of a 10 MW semi-submersible floating wind turbine under waves and wind using hybrid method to integrate the rotor thrust and moments”,

- Wind Energy Science , Vol. 7, No. 5, p. 2149-2161
- Wan, L., Gao, Z., Moan, T. and Lugni, C., 2016, “Comparative experimental study of the survivability of a combined wind and wave energy converter in two testing facilities”, *Ocean Engineering*, 111, pp.82-94. <https://doi.org/10.1016/j.oceaneng.2015.10.045>
- Wang, Y., Lin, J., Zhang, J., 2022, “Investigation of a new analytical wake prediction method for offshore floating wind turbines considering an accurate incoming wind flow”, *Renewable Energy*, Vol 185, pp 827–849
- Wen, B., Tian, X., Dong, X., Li, Z., Peng, Z., Zhang, W., Wei, K., 2020, “Design approaches of performance-scaled rotor for wave basin model tests of floating wind turbines”, *Renewable Energy*, Vol. 148, pp. 573-584
- Wen, B., Jiang, Z., Li, Z., Peng, Z., Dong, X., Tian, X., 2022, “On the aerodynamic loading effect of a model Spar-type floating wind turbine: An experimental study”, *Renewable Energy*, Vol. 184, pp. 306-319
- Werle, M. J. (2010). Wind Turbine Wall-Blockage Performance Corrections. *Journal of Propulsion and Power*, 26(6), 1317–1321. <https://doi.org/10.2514/1.44602>
- Wu, H., Fernandes, A. C., Cao, R., & Wang, E. (2023). Performance evaluation and shape improvement of a novel vertical-axis autorotation current turbine. *Ocean Engineering*, 284, 115086. <https://doi.org/10.1016/j.oceaneng.2023.115086>
- Xiaoming, R., Leroy, V., Bachynski-Polić, E. E., 2023, “Hydroelastic response of a flexible spar floating wind turbine: Numerical modelling and validation”, *Ocean Engineering*, Vol. 286, p. 115635.
- Xu, S., Xue, Y., Zhao, W., Wan, D., 2022, “A review of high-fidelity computational fluid dynamics for floating offshore wind turbines”, *Journal of Marine Science and Engineering*, Vol 10(10), 1357
- Yeo, E. J., Kennedy, D. M., & O’Rourke, F. (2022). Tidal current turbine blade optimisation with improved blade element momentum theory and a non-dominated sorting genetic algorithm. *Energy*, 250, 123720. <https://doi.org/10.1016/j.energy.2022.123720>
- Yang, J., He, Y.-P., Zhao, Y.-S., Shao, Y.-L., Han, Z.-L., 2021, “Experimental and numerical studies on the low-frequency responses of a spar-type floating offshore wind turbine”, *Ocean Engineering*, Vol. 222, p. 108571
- Zhang, D., Guo, P., Cheng, Y., Hu, Q., & Li, J. (2023). Analysis of blockage correction methods for high-solidity hydrokinetic turbines: Experimental and numerical investigations. *Ocean Engineering*, 283, 115185. <https://doi.org/10.1016/j.oceaneng.2023.115185>
- Zhang, L., Li, Y., Xu, W., Gao, Z., Fang, L., Li, R., Ding, B., Zhao, B.; Leng, J., He, F., 2022, “Systematic analysis of performance and cost of two floating offshore wind turbines with significant interactions”. *Applied Energy*, Vol 321, 119341
- Zhang, Y., Zhang, Z., Zheng, J., Zheng, Y., Zhang, J., Liu, Z., & Fernandez-Rodriguez, E. (2023). Research of the array spacing effect on wake interaction of tidal stream turbines. *Ocean Engineering*, 276.
- Zilic de Arcos, F., Tampier, G., & Vogel, C. R. (2020). Numerical analysis of blockage correction methods for tidal turbines. *Journal of Ocean Engineering and Marine Energy*, 6(2), 183–197. <https://doi.org/10.1007/s40722-020-00168-6>